Università degli studi di Napoli Federico II

Scuola politecnica e delle scienze di base

Dipartimento di Ingegneria Chimica, dei Materiali e della produzione industriale D.I.C.M.A.P.I.

Ph.D in Ingegneria dei Materiali e delle Strutture

XXVII Ciclo

A NEW HUMAN SKIN EQUIVALENT MODEL AS IN VITRO TESTING PLATFORM FOR BIOACTIVE MOLECULES

Borsa di studio finanziata da P.O. CAMPANIA FSE 2007/2013 D.G.R.

Ph.D Tesi

Scamardella Sara

TUTOR
Prof. Dr Paolo A. Netti

COORDINATORE
Prof. Dr Giuseppe Mensitieri

TUTOR AZIENDALE
Marida Bimonte Ph.D

ADVISORS
Giorgia Imparato Ph.D
Francesco Urciuolo Ph.D

2015

Alla mia famiglia, a Fabio e
alla vita che verrà

TABLE OF CONTENTS

ABBREVIATIONS

3D HSE 3D……3D human skin equivalent model
3D_HDE……3D-human dermis equivalent model
BSA ..……..bovine serum albumine
ECM ……extra-cellular matrix
GLCM ……..…gray-level co-occurrence matrices
GPMs ……gelatin porous microbeads
H/E.……....hematoxylin-eosin
HA ……hyaluronic acid
HD-µTPs …….human dermis microtissue precursors
HDF ……..…….human dermal fibroblasts
IF ……immunofluorescences analyses
MMPs ……...matrix metalloproteinases
MPM ……..…multi-photon microscopy
PBS …….phosphate-buffered saline
PSR ……..……..picro sirius red
SEM …….scanning electron microscopy
SHG …….second harmonic generation signal
UVA ……,…Ultraviolet A

Abstract

The aim of this PhD thesis is the realization of an in vitro human skin model and its validation as platform for testing bioactive molecules. Due to its endogenous nature the human skin equivalent realized was able to recapitulate both physiological and pathological status of the human skin. As consequence it has been used for recapitulating the typical UVA-induced skin alterations and to test the efficacy of photoprotectants. The thesis has been organized as follow: chapter 1 deals with a critical analysis of the literature reporting an overview of the existing human skin equivalent model highlighting their importance as alternative to animal model for testing the irritancy and toxicity of several bioactive compounds. This is a very important point, since the EU Directive prohibits the use of animals in cosmetic testing for certain endpoints, and in general strongly dictate the reduction of animal testing.

In the chapter 2 the realization of 3D dermis equivalent completely made up of endogenous extracellular matrix has been reported. The dermis is the connective part of the skin, we realized it by assembling functional microtissues precursor and demonstrate the presence of all dermis matrix components by histological and immunohistochemical analyses.

In the chapter 3 the 3D human dermis equivalent model has been used to quantify photoaging damage induced by UVA irradation to cells and extra-cellular matrix (ECM) and to evaluate bioactivity of cosmetic compounds. To this aim, matrix metalloproteinases (MMPs), collagen and hyaluronic acid (HA) synthesis -as well as collagen organization remodeling- have been investigated by immunofluorescence, histological and second harmonic generation (SHG) imaging. The results indicate that, despite to the existing model consisting in fibroblasts-populated exogenous matrix, the endogenous dermal equivalent developed is a

unique model to investigate and quantify *in vitro,* the alterations in the structure and assembly of the ECM due to photoaging.

In chapter 4 is reported the bio-fabrication of a skin full thickness in vitro model. After a first morphological characterization, through histological and immunofluorescence analysis, the model has been used as *in vitro* screening tool. A photodamage due to UVA has been induced as reported in the chapter 4, and the damage on both dermal and epidermal part of the skin has been assessed. Finally the effect of a cosmetic compound has been tested. Our results reported that the model is able to recapitulate several events typical of in vivo photoaging (collagen reduction, MMP overexpression and cellular damage such as reduction of Ki67 and P63 expression). We speculated that due to its endogenous nature the skin model realized is able to recapitulate a more physiological microenviroment for cell and tissue development compared to existing fibroblasts-populated exogenous matrix.

Moreover we hypothesized that the human skin model realized could be used not only in vitro but also *in vivo* as skin substitute in clinical application.

Chapter 1

In vitro skin models as a testing platform: an overview

Introduction

Skin is the largest organ of human body and is responsible for the protecting the body from the environment. However, when this barrier is disrupted, as in the case of large wounds, burns, and chronic, diabetic ulcers, the clinical use of grafted skin has shown therapeutic efficacy. However, such skin autografts are limited by healthy donor site availability. As a result, many approaches have been explored for skin replacement therapy, including cadaver skin. While these options offer temporary benefit, they only persist at the grafting site for a limited amount of time. In response to these limitations, new approaches for skin engineering have been tested and developed in last years.

These advances have led to the development of in vitro models to study wound healing, skin cancer, and skin biology. Since skin barrier function is recapitulated in these in vitro skin equivalents, they are now an important part of consumer product testing. For example, since the European Union will no longer allow the sale of new consumer products tested on animals, it is essential that Companies developing consumer products who wish to sell them abroad must find alternative modes of testing that avoids the use of animals. In order to replace animal testing, engineered skin needs to closely mimic the complexity of the in vivo tissue and must respond to toxic and no toxic agents in a fashion that mimics native skin [1].

Skin: structure and function

The human skin is the largest organ of the body, making up 16% of body weight, with a surface area of 1.8m^2. It has several functions, the most important being to form a physical barrier to the environment, allowing and limiting the inward and outward passage of water, electrolytes and various substances while providing protection against micro-organisms, ultraviolet radiation, toxic agents and mechanical insults (see Table 1). However, damaged skin cannot perform these critical functions and numerous complications how infection or fluid loss can occur.

Table 1. Functions of the skin.

- Provides a protective barrier against mechanical, thermal and physical injuryandnoxious agents.
- Prevents loss of moisture.
- Reduces the harmful e€ects of UV radiation.
- Acts as a sensory organ.
- Helps regulate temperature control.
- Plays a role in immunological surveillance.
- Synthesises vitamin D3 (cholecalciferol).
- Has cosmetic, social and sexual associations.

Starting from the surface and reaching deep into the human skin consists by an epithelium, the epidermis; by a connective tissue, *dermis* and by an adipose tissue called subcutaneous (fig.1).

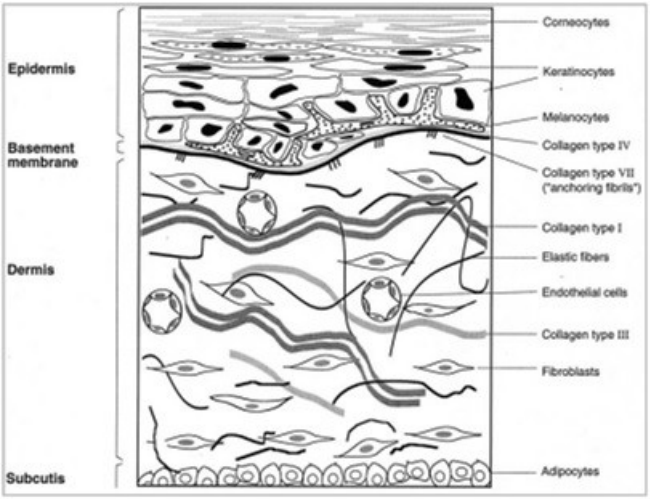

Figure 1 : Scheme of different layers of the human skin [2].

Epidermis

The epidermis is the outer layer, serving as the physical and chemical barrier between the interior body and exterior environment, maintaining physiological homeostasis [3].

The epidermis is stratifed squamous epithelium. The main cells of the epidermis are the keratinocytes, which synthesise the protein keratin. Protein bridges called desmosomes connect the keratinocytes, which are in a constant state of transition from the deeper layers to the superfcial. The four separate layers of the epidermis are formed by the differing stages of keratin maturation [4]. The epidermis varies in thickness from 0.05 mm on the eyelids to 0.8±1.5 mm on the soles of the feet and palms of the hand. Moving from the lower layers upwards to the surface, the four layers of the epidermis are (fig.2):

_ stratum basale (basal or germinativum cell layer)

_ stratum spinosum (spinous or prickle cell layer)

_ stratum granulosum (granular cell layer)

_ stratum corneum (horny layer).

In addition, the stratum lucidum is a thin layer of translucent cells seen in thick epidermis. It represents a transition from the stratum granulosum and stratum corneum and is not usually seen in thin epidermis. Together, the stratum spinosum and stratum granulosum are sometimes referred to as the Malphigian layer.

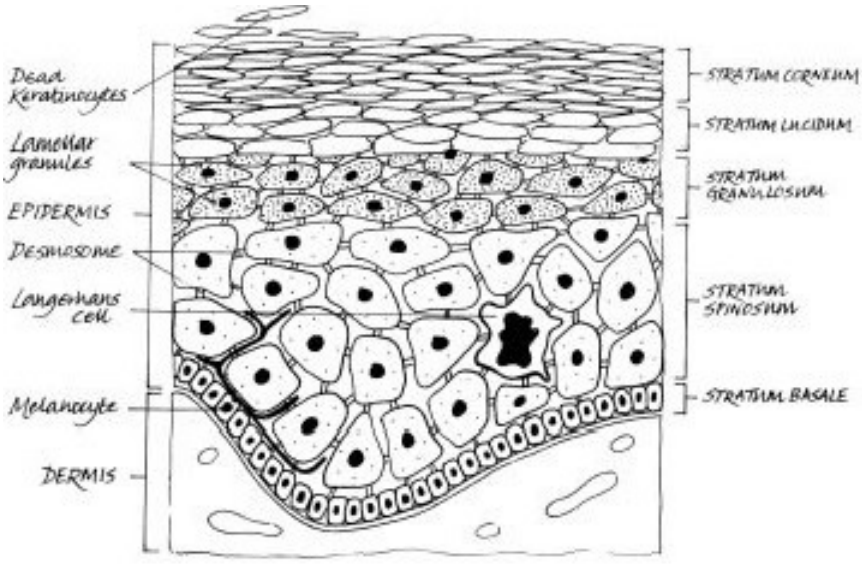

Figure 2. Layers of the epidermis.

Stratum basale

The innermost layer of the epidermis which lies adjacent to the dermis comprises mainly dividing and non-dividing keratinocytes, which are attached to the basement membrane by hemidesmosomes. As keratinocytes divide and differentiate, they move from this deeper layer to the surface. Making up a small proportion of the basal cell population is the pigment (melanin) producing melanocytes. These cells are characterised by dendritric processes, which stretch between relatively large numbers of neighbouring keratinocytes. Melanin accumulates in melanosomes that are transferred to the adjacent keratinocytes where they remain as granules. Melanin pigment provides protection against ultraviolet (UV) radiation; chronic exposure to light increases the ratio of

melanocytes to keratinocytes, so more are found in facial skin compared to the lower back and a greater number on the outer arm compared to the inner arm.

The number of melanocytes is the same in equivalent body sites in white and black skin but the distribution and rate of production of melanin is different.

Intrinsic ageing diminishes the melanocyte population.

Merkel cells are also found in the basal layer with large numbers in touchsensitive sites such as the fingertips and lips. They are closely associated with cutaneous nerves and seem to be involved in light touch sensation.

Stratum spinosum

As basal cells reproduce and mature, they move towards the outer layer of skin, initially forming the stratum spinosum. Intercellular bridges, the desmosomes, which appear as `prickles' at a microscopic level, connect the cells. Langerhans cells are dendritic, immunologically active cells derived from the bone marrow, and are found on all epidermal surfaces but are mainly located in the middle of this layer. They play a significant role in immune reactions of the skin, acting as antigen-presenting cells.

Stratum granulosum

Continuing their transition to the surface the cells continue to flatten, lose their nuclei and their cytoplasm appears granular at this level.

Stratum corneum

The final outcome of keratinocyte maturation is found in the stratum corneum, which is made up of layers of hexagonal-shaped, non-viable cornified cells known as corneocytes. In most areas of the skin, there are 10±30 layers of stacked corneocytes with the palms and soles having the most. Each corneocyte is surrounded by a protein envelope and is filled with water-retaining keratin proteins. The cellular shape and orientation

of the keratin proteins add strength to the stratum corneum. Surrounding the cells in the extracellular space are stacked layers of lipid bilayers.

The resulting structure provides the natural physical and water-retaining barrier of the skin. The corneocyte layer can absorb three times its weight in water but if its water content drops below 10% it no longer remains pliable and cracks. The movement of epidermal cells to this layer usually takes about 28 days and is known as the epidermal transit time.

Dermoepidermal junction/basement membrane

This is a complex structure composed of two layers. The structure is highly irregular, with dermal papillae from the papillary dermis projecting perpendicular to the skin surface. It is via diffusion at this junction that the epidermis obtains nutrients and disposes of waste. The dermoepidermal junction flattens during ageing which accounts in part for some of the visual signs of ageing.

Dermis

Under the epidermis, connected to it by the dermal-epidermal junction, is localized the *dermis*, a dermal connective tissue which contains extracellular matrix proteins such as collagen, primarily collagen of type I and in lesser amounts of type III, elastic fibers, fibronectin, laminin and proteoglycans which are produced and secreted into the extracellular matrix by fibroblasts, the primary cell type of the *dermis* [5].

The dermis varies in thickness, ranging from 0.6 mm on the eyelids to 3 mm on the back, palms and soles. It is found below the epidermis and is composed of a tough, supportive cell matrix. Two layers comprise the dermis:

_ a thin papillary layer

_ a thicker reticular layer.

The papillary dermis lies below and connects with the epidermis. It contains thin loosely arranged collagen fibres. Thicker bundles of

collagen run parallel to the skin surface in the deeper reticular layer, which extends from the base of the papillary layer to the subcutis tissue.
Collagen fibres make up 70% of the dermis, giving it strength and toughness. Collagen is the most abundant protein in dermal connective tissue and is mainly seen as structural protein. Collagens consist of three polypeptide chains. These are super-coiled around a central axis in a right-handed manner to form a triple helix. Collagen molecules self-assemble into collagen fibers, which form collagen bundles after cross-linking [6]. During the biosynthesis of collagen, the molecule undergoes several post-translational modifications. Depending on their structure and supra-molecular organization, collagens can be classified into fibrillar (accounting for 90% of all collagens) and non-fibrillar collagens. For example, fibrillar collagens are responsible for conferring tension and provide support and structural integrity of the skin [7, 8]. In contrast, basement membrane collagens such as collagen type IV are more flexible, giving the basement membrane its typical characteristics.
Elastin is a fibrous protein, hard and stable responsible of the elastic properties of connective tissue Elastic fibers have a central core of amorphous, hydrophobic cross-linked, elastin surrounded by a tubular shell fibrillary proteins. Elastic fibers are a minor component and play a functional role in resisting deformational forces and providing the skin's elasticity by forming a fine network [5]. In short, collagen and elastin may be considered as the bricks of extra-cellular matrix due to their contribution to the mechanical properties of ECM.
Proteoglycans are also non-collageneous proteins similar to elastic fibers and comprising only a small percentage of skin and provide viscosity and hydration. They are responsible for the assembly of the extracellular matrix and regulates the diameter and structure of collagen fibrils, thus preventing abnormal fibril assembly [9]. Two of the most common proteins responsible for cell adhesion are fibronectin and laminin.

Fibronectin is the second most abundant protein in ECM, where it is organized into a fibrillar network. It is a large glycoprotein dimer and each monomer contains three types of repeating units designated type I, II and III. In these units we can find functional domains responsible for interaction with cell surface receptors and with fibronectin itself. Laminin is a complex adhesion molecule especially found in the basement membrane of almost every tissue. These various extracellular matrix proteins in the dermal connective tissue mainly contribute to the maintenance of skin integrity and architecture. Therefore, damages to the dermal connective tissue by the aging process can be connected to structural changes of the skin as wrinkling, loss of elasticity, sagging and laxity.

Tissue Engeenering of skin

Tissue engineering is an interdisciplinary field of the regenerative medicine, focused on the creation of tissues and organs with biomaterials and nanostructures to develop, sustain and repair an organ or tissue function. The main goal is to mimic the normal structure of a tissue. Cells and ECM are used to develop biological substitutes to be assimilated by the body during the tissue regeneration, and cells can also be used in a cell therapy procedure. To achieve these goals, an artificial (ECM) and a source of cells are required as well as growth factors (fig. 3)[10]. Tissue engineered replacements play an important role in the treatment of skin wounds, but they are also an option for the treatment of several skin disorders affecting the patients' general appearance and self-esteem; in these cases, skin substitutes and cell therapies may have important clinical applications.

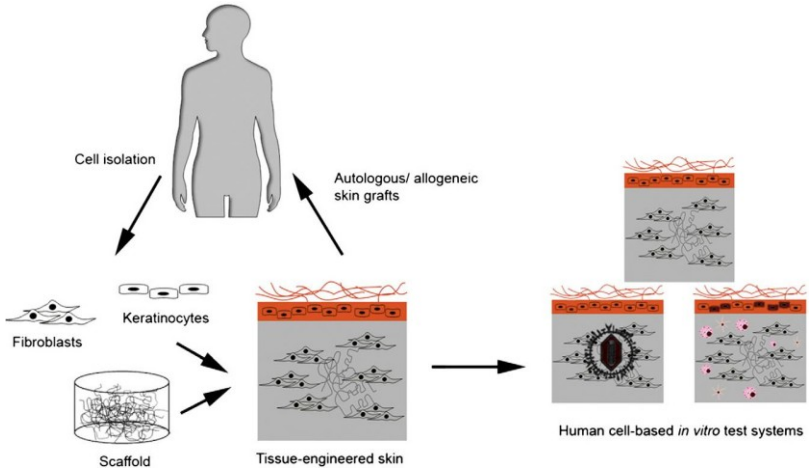

Figure 3: Basic principles of Tissue Engeenering: Primary keratinocytes and fibroblasts are isolated from human donor tissues, which are then *in vitro* expanded prior seeding onto suitable scaffold materials/matrices. For a full-thickness skin equivalent, the fibroblasts and the matrix are initially used to establish the dermal part. The keratinocytes are seeded afterwards on the top of the dermis to ultimately form the epidermal part of the skin substitute. The *in vitro*-engineered skin can serve as skin graft or can be used as human-cell based *in vitro* test system.[11]

However, besides their use as *in vivo* grafts, recently, other applications have emerged for skin substitutes as *in vitro* test systems [12]. In this context, they enable not only the investigation of fundamental processes in the skin, but also the hazard assessment of various chemical or dermatological compounds that are topically applied on the skin without the need to use animal models.

In fact, the increased awareness of animal welfare within the general public and the scientific community has stimulated recent advances toward the development of commercial and noncommercial in vitro human skin equivalent (HSE) models. The need for alternative models to assess dermal toxicity is great in biomedical research to test or evaluate the toxicity of numerous compounds. Although these in vitro models may serve as alternatives, they cannot completely satisfy the physiological or anatomical requirements found in in vivo models. In order to reduce or

replace animals in scientific research, ‘‘animal alternatives’’ are being pursued.

These HSE cell culture models have been used to study percutaneous absorption, metabolism [13] , and toxicology [14].

A number of pharmaceutical and cosmetic companies are using in vitro models to assure the safety of their products and to meet regulatory requirements to classify irritancy potential. In addition, these results are combined with other in vitro biochemical tests to determine the safety of the product.

Today, in vitro reconstructed skin models are used globally in both industrial and academic research laboratories. In general terms, the implementation of these three-dimensional (3D) *in vitro* reconstructed human tissue models makes it possible for

pharmaceutical, chemical and cosmetical product companies to:

- ✓ test the efficacy of newly developed formulations and products and thus to use them for claim support,
- ✓ reproducibly differentiate compounds that cause reversible and irreversible toxicity without resorting to *in vivo* animal testing,
- ✓ provide accurate and measurable mechanistic information that can be utilized to determine whether a molecule or compound can be altered to reduce irritation or toxicity, without loss of efficacy,
- ✓ objectively compare the toxicity and efficacy of newly developed compounds with those already in use in the market place for the same purpose,
- ✓ reveal the precursor steps which lead to toxic reactions, thereby making reformulations possible, based on human response,
- ✓ evaluate the long term stability or shelf-life of finished products or raw materials,
- ✓ determine the potential health risks of employees exposed to chemicals (worker safety) [15].

The importance of skin in vitro model: Cosmetics Directive and Regulation

The cosmetic industry is complex. More than ever, manufacturers and distributors are facing new legislation. As innovative cosmetics as well as the technology behind them emerges and advances through new studies and research, so too does the demand for governance. But deciphering the demands of legislation can be challenging.

In recent years national and European legislation has placed considerable constraints on industry to totally abandon animal-based test systems when assessing the toxicological potential of chemicals and finished products. Both the REACH directive (Registration, Evaluation, Authorization and Restriction of Chemicals), the Classification, Labeling and Packaging (CLP) directive and the EU Cosmetics directive demand for alternatives to animal testing. Hence they are creating a growing need for human reconstructed skin models, accelerating the adoption of these models in skin-related testing strategies required for regulatory purposes [16].

In the EU, regulations applied to cosmetic products are EU Cosmetic Directive (76/768/EEC) and the EU Cosmetic Regulation (EC 1223/2009).

A Directive, by definition, is a legislative act that serves to direct, indicate or guide. A directive in the EU represents a guide that every member country has to transpose into its national legislation. However, because some countries are stricter than others about adoption of laws, sometimes rules are not equally applied everywhere as intended, resulting in the need to draft multiple versions of the directive specific to each country.

A Regulation is a legislative act that imposes clear and detailed rules. A regulation is not required to be incorporated into the national laws, but is immediately enforceable in all member states. Keep in mind as well the

fact that a regulation only needs to be translated into the national language of the 27 EU member state.

The EU Cosmetic Directive (76/768/EEC) was originally issued on July 27, 1976 as an initial means of ensuring the safe sale [17] and distribution of cosmetic products within the EU Community market. With a primary goal of protecting overall consumer health, the Directive included rules on the composition [18], labeling and packaging of cosmetic products. Thus, the responsibility for product safety lies with the cosmetic manufacturer or the legal person placing a cosmetic product on the Community market, who must be able to demonstrate that the product is safe for the consumer. But as the cosmetic industry advanced utilizing new, ground-breaking technologies and innovations, the legislation supporting it needed to change / evolve too.

The *Cosmetic Regulation 1223/2009* was adopted on the 30th of November 2009 to essentially replace the EU Cosmetic Directive. The regulation was created to implement a more robust approach at enforcing product safety and is immediately enforceable because there is no transposition into the laws of individual countries, and only translation into the languages of the EU member countries is required.

The new EU Regulation 1223/2009 (Cosmetics Regulation) has been in force since 11 July 2013. It strengthens the safety of cosmetic products and streamlines the framework for all operators in the sector. The Regulation simplifies procedures to the extent that the internal market of cosmetic products is now a reality.

The new Regulation replaces Directive 76/768/EC*,* and had been substantially revised on numerous occasions. It provides a robust, internationally recognised regime, which reinforces product safety while taking into consideration the latest technological developments, including the possible use of nanomaterials. The previous rules on the ban of animal testing were not modified.

The Cosmetics Directive provides the regulatory framework for the phasing out of animal testing for cosmetics purposes.

Specifically, it establishes:

- ✓ Testing ban – prohibition to test finished cosmetic products and cosmetic ingredients on animals;
- ✓ Marketing ban – prohibition to market finished cosmetic products and ingredients in the EU which were tested on animals.

The testing ban on finished cosmetic products applies since 11 September 2004; the testing ban on ingredients or combination of ingredients applies since 11 March 2009.

The marketing ban applies since 11 March 2009 for all human health effects with the exception of repeated-dose toxicity, reproductive toxicity, and toxicokinetics. For these specific health effects, the marketing ban applies since 11 March 2013, irrespective of the availability of alternative non-animal tests.

The beginnings of Human Skin models

One of first commercially available models was produced by Organogenesis, Canton, MA, USA and was called LSE (Living Skin Equivalent) and later Testskin I and II. This skin model was originally developed in 1991 [19, 20] and consisted of a differentiated epidermal tissue produced on a collagen lattice populated with human fibroblasts. Various test applications were developed using this skin construct including UV irradiation [21], skin irritation [22, 23], and dermal absorption [24].

At approximately the same time, another US based company called Advanced Tissue Sciences, La Jolla, CA, USA, launched a set of *in vitro* reconstructed human skin models under the brand name ‘Skin²TM. These full-thickness (dermis/epidermis) skin models called ‘Skin²TM ZK1300 and ZK1350 were shipped worldwide and evaluated thoroughly, both morphologically and biochemically [25, 26], and used in a wide

range of toxicological applications. These included skin corrosion for which regulatory approval was obtained by the US Department of Transportation (27), phototoxicity [28, 29, 30, 31], skin irritation [32, 33, 34, 35] and dermal absorption [36, 37, 38, 3]. Unfortunately, despite the multiple successful validation efforts, the company's shareholders decided to withdraw from the *in vitro* skin business in 1995 and focus entirely on the clinical skin equivalent called Dermagraft-TC, which was developed as a temporary wound cover for burn patients.

Commercially available skin models today

Today a variety of 3D in vitro reconstructed human skin model are commercially available on a routine basis.

Some were already developed in the early 1990's including the EpiSkin™ model (L'Oréal, Lyon, France) and EpiDerm™ model (MatTek Corporation, MA, USA). Subsequently, additional human skin models were introduced to the commercial market, including the RHE or Reconstructed Human Epidermis (SkinEthic, Lyon, France), the EST1000® skin model (CellSystems, Troisdorf, Germany), the Phenion® Full-Thickness Skin Model and OSREp (Open Source Reconstructed Epidermis) model (Henkel, Düsseldorf, Germany), the Straticell model (Straticell, Les Isnes, Belgium), the StrataTest® model (Stratatech, Madison, WI, USA) and the more recently introduced Labcyte model (Gamagori, Japan) and Vitrolife-Skin™ model (Kyoto, Japan).

The EpiSkin™ and SkinEthic RHE™ skin models

The EpiSkin™ (fig.4) model was originally developed by E. Tinois in 1991 and is composed of a collagen lattice containing human fibroblasts, surfaced with a film of type IV collagen, overlaid with a fully differentiated human epidermis (40).

The models were initially produced by the company Imedex (Lyon, France), that became acquired by L'Oréal in 1997. The SkinEthic RHE™ model was developed by M. Rosdy in 1990. This epidermal construct generated by seeding human keratinocytes on inert synthetic filters, which are consequently exposed to the air-liquid interface and maintained using a chemically defined culture medium (41). The model became commercially available in 1993 by SkinEthic Laboratories, which also was acquired by L'Oreal (in 2006). Today, both the EpiSkin™ and SkinEthic RHE™ (fig 4)(Reconstructed Human Epidermis)models are being produced by SkinEthic Laboratories, Lyon, France.

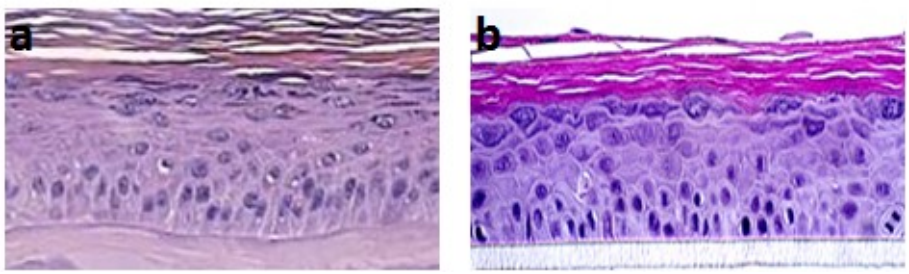

Figure 4: Histological Hematoxylin-eosin staining of cross-section. (a) EpiSkin™ and (b) and SkinEthic RHE™ model.

The EpiSkin™ and SkinEthic RHE™ models have been scientifically validated for skin corrosivity and skin irritation assessment by ECVAM [42, 43]. In addition, EpiSkin™ and SkinEthic RHE™ are also useful models for screening acute and chronic skin irritation of topical formulations [44], for testing the phototoxicity of raw materials or finished products [45, 46], for screening the genotoxicity potential of topically

applied compounds or formulations [47], for ranking the skin permeability and metabolism of products [48], for understanding the effects of UVA and UVB irradiation and UVB protection [49], dermal penetration [50] and for detecting the genomic and transcriptomic signatures [51], for contact allergy profiles [52].

The EpiDerm™ and Epiderm-FT™ skin models

The EpiDerm™ in vitro reconstructed skin model, produced by MatTek Corporation, Ashland, MA, USA was originally developed by J. Kubilus and M. Klausner. This model is also composed of human epidermal keratinocytes that develop a fully-differentiated epidermal tissue (fully differentiated natural epidermis displaying a basement membrane, proliferating keratinocytes and a stratum corneum) after air-liquid interface cultivation on inert polycarbonate membranes (fig. 5-a). The EpiDerm™ model was introduced to the commercial market in 1993 and was first described by Cannon *et al*, [53]. Later MatTek introduced a full-thickness model called EpiDerm-FT™ that featured both epidermal and dermal layers (fig 5-b) [54].

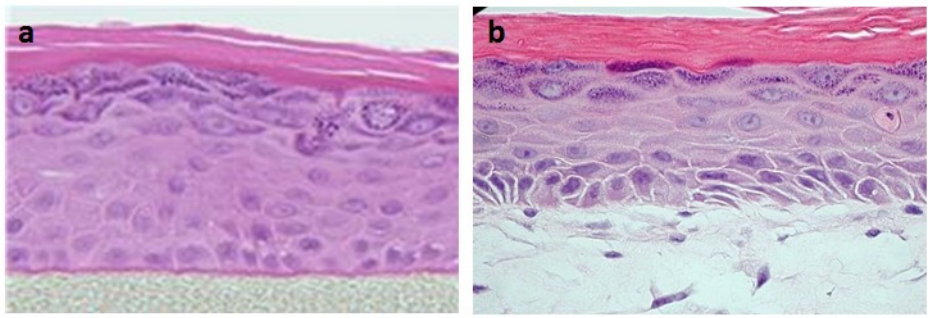

Figure 5: Histological Hematoxylin-eosin staining of cross-section. (a) EpiDerm™ and (b) and EpiDerm-FT™ model.

Shortly after, a melanocyte containing epidermal model called MelanoDerm™ [55] was developed.

For 15 years, the company has consistently mass-produced, in a highly reproducible way, the EpiDerm™ tissues [56].

The EpiDerm™ models are used by several industries in product development, claims substantiation, safety assessment and drug discovery and have been involved in several regulatory validation studies. These include skin corrosion [57, 58] and skin irritation [59,60] for which the model obtained regulatory approval as full replacement method, and are referenced in the OECD TG 431 (skin corrosion) and OECD TG 439 (skin irritation). In addition, as demonstrated in two independent studies, *in vitro* skin irritation data obtained with the EpiDerm™ model correlate well with human dermal irritation effects caused by cosmetics and chemicals [61, 62]. Also pre-validation studies on phototoxicity [63, 64] and dermal penetration validation studies [65, 66] have been performed. A variety of additional testing applications using the EpiDerm™ models include cosmetic products testing [61], skin metabolism [67-68] genotoxicity [69], nanotoxicity [70,71], and pharmacology [72].

The EST1000® skin model

The EST1000® skin model is an *in vitro* 3D reconstructed human epidermal model produced by Cell Systems, Troisdorf, Germany. This model has been commercially

available since 2004 and is used in a wide range of regulatory toxicology tests (e. g., irritation, corrosion and phototoxicity studies). EST1000® was validated successfully

and obtained regulatory approval for skin corrosion testing in accordance with the OECD test guideline 431 [73]. Currently the EST1000® model is undergoing validation for skin irritation. In addition, the model was assessed for its utility in skin sensitization testing [74] and is currently taking part in a pre-validation study for skin sensitization (personal communication). Other applications of both EST1000® model include phototoxicity and genotoxicity [75, 76, 77]. Very recently the name of the EST1000® model was changed into epiCS®.

The Phenion® Full-Thickness Skin Model and the OS-Rep model

The proprietary Phenion® Full- Thickness Skin Model (Phenion® FT model) was originally developed by scientists of the Henkel AG & Co. KGaA (Düsseldorf, Germany) in collaboration with the Universities of Frankfurt and Munich, and was introduced commercially in 2006. Human fibroblasts isolated from biopsies obtained from healthy donors are grown in a specially-produced stable matrix equivalent. After the development of this dermal equivalent, keratinocytes originated from the same donor are seeded on top. Within several days an epidermal tissue featuring all typical epidermal layers including a multilayered stratum corneum develops.

The Phenion® Full-Thickness Skin Model exhibits structural and physiological properties comparable with native human skin [78]. It is primarily used for efficacy studies, skin irritation [79], phototoxicity [80], dermal absorption [81], metabolism [82] and genotoxicity studies [83]. Henkel also launched the so-called ‘Open Source Reconstructed Epidermis’, or OSREp model. The Open Source concept supports the idea of free public access to information and systems, currently best known in the computer software market. When applied to skin models “Open Source” means that, once a production method has been established, the know how becomes openly available in order to empower scientific groups throughout the world to produce the model ‘internally’, independent of any commercial supplier [84]. The idea of a protocol for epidermal model production which can be applied by any experienced user was first introduced by Poumay *et al.* [85]. Based on this protocol, which was optimized by Henkel regarding medium composition and cell quality, the OS-REp model was established, featuring basic epidermal characteristics [86,87]. In addition, to expand the scientific knowledge base of this model, it is

intended to be used for the toxicological assessment of substances, thus making it a viable alternative to animal testing. Clearly, especially for regulatory purposes, validated SOP's and quality criteria for both OS model production as well as testing protocol have to be strictly respected. Recently the OS-Rep model underwent a successful catch-up validation for skin irritation assessment, which has been submitted to EURL-ECVAM for official regulatory acceptance [88].

The StratiCELL® skin model

The company Straticell, Les Isnes, Belgium, founded in 2005 as spin-out of the University of Namur, Belgium, has developed two proprietary *in vitro* skin models. The StratiCELL® reconstituted human epidermis with and without pigmentation, is composed of normal human keratinocytes and melanocytes cultured in a well-defined

serum-free medium on a polycarbonate filter at the air-liquid interface. In addition, the company provides epidermal models from young/old & normal/diseased individuals (atopic dermatitis and psoriasis). Currently, the StratiCELL® skin model is preparing for catch-up skin irritation validation and the models were also evaluated for usefulness in nanotoxicology testing [89]. Additional specific safety applications of the StratiCELL® skin model, for assessing genotoxicity and phototoxicity are currently being evaluated.

The StrataTest® skin model

The StrataTest® human skin model, developed and commercialized by the company Stratatech, Madison, WI, USA, is a fully-stratified, multi-layered human skin tissue
composed of both epidermal and dermal components. The epidermal compartment is generated by the terminal differentiation of NIKS® keratinocytes, a spontaneously
immortalized cell line, which serves as a unique, consistent and unlimited source of human keratinocyte progenitors [90]. The dermal compartment of the model contains
normal human dermal fibroblasts distributed throughout a fibrous collagen matrix. The NIKS® cells are nontumorigenic, pathogen-free, and have been clinically.
evaluated as the epidermal component of StrataGraft® skin substitute tissue [91]. Unlike skin models that must replenish keratinocyte sources periodically as stocks are depleted or utilize cells pooled from multiple donors, a uniform keratinocyte source is used to manufacture the StrataTest® human skin model. This provides a consistent, reproducible test platform. Several studies have described the biological response of NIKS®- generated models to chemical compounds [92], antibiotic formulations [93], and surfactants [94], signaling proteins [95], and environmental factors including hypoxia [96, 97], ozone, cigarette smoke, and ultraviolet light [98]. An additional unique feature of the NIKS® keratinocytes resides in their ability to be genetically-modified by non-viral means to generate stably-transfected clones [99, 100]. In vitro skin irritation data generated with the StrataTest® model are comparable to human in vivo scores [101].
Currently the model is preparing for catch-up skin irritation validation.

The LabCyte™ skin model

The LabCyte™ skin model (EPI-model) is produced by Japan Tissue Engineering Co., Ltd., Gamagori, Japan,by culturing human epidermal cells on inserts. After human epidermal cells have proliferated, exposure to the air-liquid intereface causes it to keratinize, creating a cultured epidermis model similar to the human epidermis [102]. The EPI-model has undergone validation for skin corrosion in accordance with the OECD test guideline 431 [103]. More recently the LabCyte™ model has undergone a formal catch-up validation study for skin irritation [104] and has been included into a new draft version of the OECD TG 439 [105].

The Vitrolife-SKIN™ skin model

The Vitrolife-SKIN™ skin model, produced by Gunze Corporation Ltd, Kyoto, Japan, is a commercially available 3D reconstructed skin model, which is supplied as a kit containing 24 collagen sponges without cells and culture medium. The models need to be prepared in the laboratory (cultivation of cells in sponges) resulting in a 3D skin model composed of a dermis and an epidermis with cornified layers as described in the literature [106, 107]. The model was recently validated for corrosivity [108, 109] and obtained the JACVAM (Japanese Centre for the Validation of Alternative Methods) validity statement that the Vitrolife-SKIN™ corrosivity assay complies with the OECD guideline TG 431 [110].

REFERENCES

1. Evangelia Bellas, ‘‘In vitro 3D Full-Thickness Skin-Equivalent Tissue Model Using Silk and Collagen Biomaterials”, Macromol. Biosci. 2012

2. Karin Scharffetter Kochanek, et al. “Photo-aging of the skin from phenotype to mechanisms.” Experimental Gerontology 35 (2000) 307–316

3. Rahaman MN, Mao JJ. “Stem cell-based composite tissue constructs for regenerative medicine.” Biotechnol Bioeng. 2005 Aug 5;91(3):261-84. Review.

4. Makrantonaki E, Zouboulis CC. “The skin as a mirror of the aging process in the human organism--state of the art and results of the aging research in the German National Genome Research Network 2 (NGFN-2).” Exp Gerontol 2007; 42(9): 879-886.

5. Bateman A, Chothia C. “Fibronectin type III domains in yeast detected by a hidden Markov model.” Curr Biol 1996; 6(12):1544-1547.

6. Oxlund H, Andreassen TT. “The roles of hyaluronic acid, collagen and elastin in the mechanical properties of connective tissues.” J Anat 1980; 131(Pt 4): 611-620.

7. Uitto J. “Connective tissue biochemistry of the aging dermis. Agerelated alterations in collagen and elastin.” Dermatol Clin 1986; 4(3): 433-446.

8. Okamoto O, Fujiwara S. “Dermatopontin, a novel player in the biology of the extracellular matrix.” Connect Tissue Res 2006; 47(4): 177-189.

9. Kligman AM, Graham JA. “The psychology of appearance in the elderly.” Clin Geriatr Med 1989; 5:213-22

10. Cristina Velasquillo et al “Skin 3D Bioprinting. Applications in Cosmetology” Journal of Cosmetics, Dermatological Sciences and Applications, 2013, 3, 85-89

11. Florian Groeber "Skin Tissue Engineering: in vivo and in vitro applications" Advanced Drug Delivery Reviews (2011), 352–366, Elsevier.

12. Hugo Fernandes,Lorenzo Moroni,"Extracellular matrix and tissue engineering applications". Journal of Material Chemistry

13. Slivka et al, "Characterization, Barrier Function, and Drug Metabolism of an In Vitro Skin Model" J Invest Dermatol 100:40-46, 1993

14. Klausneret et al "UVB irradiation of an organotypic skin model, Epidermy, results in significant release ofcytokines". Toxicologist, 15:325, 1995

15. Bart de wever," overview of human three-dimensional(3D) skin models used for dermal toxicity assessment". *Household and Personal Care Today, Vol. 8 nr. 1 January/February 2013*

16. *Saliner, patlewixz& P.Worth "Review of Literature-Based Models for Skin and Eye Irritation and Corrosion" Rur 22320 EN, 2006*

17. European Economic Community Council Directive 76/768/EEC of 27jule 1976 on the approximation of the laws of the Member states relating to cosmetic products. *Official Journal of European Communities* L 262, 27/9/1976, p. 169. Update: 7th amendment by Directive 2003/15/EC of the European Parliament and of the Council of 27 February 2003; Commission Directive 2005/80/EC of 21 November 2005 amending Council Directive 76/768/EEC, concerning cosmetic products, for the purposes of adapting Annexes II and III thereto to technical progress*. Official Journal of European Communities L 303,* 22/11/2005 pp. 0032 –0037.

18. ECVAM (2004) Report for establishing the timetable for phasing out animal testing for the purpose of the cosmetics directive.

19. N. Parenteau, C. Nolte et al., *J Cell Biochem*. 45(3):245-51,1991

20. N.Parenteua, P. Bilbo et al., *Cytotechnology* 9(1-3):163-171,1992.

21. Y. Tanasguchi, K. Suzuki, et al.,. *J Toxicol Sci*. 19(1):37-44, 1994.

22. T. Watanabe, T. Hasegawa et al., *Pharm Res*., 19, 5, 669-675,2002

23. K. Sugibayashi, T. Watanabe et al., *Toxicol*. *in Vitro* 16(6):759-763, 2002.

24. A. Ernesti, M. Swiderek, *Skin Pharmacol*. 5(3):146-153, 1992

25. P. Stoppie, P. Borghgraef et al., *Eur J Morphol*. 31(1-2):26-9, 1993.

26. B. De Wever, L. Rheins. *Cosmetics and Toiletries Manufacture Worldwide* 240-248, 1995.

27. M. Liebsch, B. Döring et al., *Toxicol. in Vitro* 9(4):557-562, 1995.

28. S. Edwards, T. Donnelly et al., *Photodermatol Photoimmunol Photomed*.10(3):11-7, 1994.

29. M. Liebsch, C. Barrabas et al., *ALTEX*. 14(4):165-174, 1997.

30. B. De Wever, *Science and Cosmetology* 34:12-26, 1995.

31. M. Liebsch, C. Barrabas et al., *ALTEX*. 14(4):165-174, 1997

32. R. Osborne, M. Perkins, *Food Chem Toxicol*. 32(2):133-42, 1994.

33. Y. Tanasguchi, K. Suzuki, et al.,. *J Toxicol Sci*. 19(1):37-44, 1994

34. P. Joller, J. Menrad et al., *Arzneimittelforschung*. 46(6):649-53,1996

35. J. Demetrulias, T. Donnelly et al., *Exp. Dermatol*. 7(1):18-26, 1998

36. B. De Wever, L. Rheins, *In Vitro Toxicology*; 121-131; Ed. A. Rougier, A. M. Goldberg and H. I. Maibach; Mary Ann Liebert, Inc. 1994.

37. A. Vickers, W. Biggi, et al., *Life Sci*., 57(3):215-24, 1995.

38. V. Keeble, L. Correll, et al., *J Appl Toxicol*. 16(5):401-6, 1996.

39. R. Lee , H. et al., *J Pharm Sci*. 11:1186-90, 1996.

40. E. Tinois, J. Tiollier et al., Exp Cell Res. 193(2):310-9, 1991.

41. M. Rosdy, C. Claus, J Invest Dermatol. 95(4):409-14, 1990

42. J. Fentem, P. Botham et al., Toxicol. in Vitro, 12, 483-527, 1998

43. OECD guideline n° 431 OECD, Paris, France, 2004

44. A.de Brugerolle de Fraissinette, V. Picarles et al., Cell Biol Toxicol., 15:121-135, 1999.

45. F. Bernard, C. Barrault et al., Cell Biol Toxicol., 16(6):391-400, 2000

46. D. Lelièvre, P. Justin, et al., Tox. In Vitro, 21(6):977- 995, 2007

47. N. Flamand, L. et al., Genetic Toxicology & Environnement Toxicology, Elsevier, 2006.

48. V. Luu-The, D. Duche, et al., J. Steroid Biochem. Mol. Biol. 116(3–5):178–186, 2009.

49. D. Bacqueville, A. Mavon, Int. J. of Cosmetic Science 31(4):293-302, 2009

50. B. Rozmana, M. Gasperlin et al., Eur J. Pharmaceutics and Biopharmaceutics, 72(1):69-75, 2009

51. K. Zakikhany, J. Naglik et al., Mol. Microbiol. (9):2938–2954, 2007

52. A. Gazel, M. et al., Journal of Cellular Physiology (217):686-692, 2008

53. C. Cannon, P. Neal et al., Toxicol. In Vitro. 8(4):889-91,1994

54. P. Hayden, J. Kubilus et al., The Toxicologist , 72(S1):158, 2003

55. G. Majmudar, G. Jacob et al., Cosmet. Science, 361-367, 1998.

56. A. Rispin, K. Stitzel, et al., Regulatory Toxicology & Pharmacology 45:97–103, 2006.

57. M. Liebsch, D. Traue, et al., ATLA 28:371–401, 2000

58. ECVAM. ESAC Statement, Corrosion Testing, 2000 http://ecvam.jrc.it/ft_doc/EpiDerm_statement.pdf

59. H. Spielmann, S. Hoffmann et al., ATLA 35: 559–601, 2007

60. H. Kandárová, P. Hayden et al., ATLA 37:671–689, 2009

61. C. Faller, M. Bracher et al., Toxicology in Vitro 16:557–572, 2002.

62. D. Jírová, D. Basketter et al., Contact Dermatitis, 62(2)109-16, 2010

63. M. Liebsch, C. Barrabas et al., ALTEX. 14(4):165-174, 1997.

64. M. Liebsch; D. Traue et al., In Alternatives to Animal Testing II: Proceedings of the Second International Scientific Conference Organised by the European Cosmetic Industry, Brussels, Belgium (ed. D. Clark, S. Lisansky & R. Macmillan), 160–166. Newbury, UK: CPL Press, 1999

65. M. Schäfer-Korting, U. Bock, et al., ATLA 34:283–294, 2006

66. M. Schäfer-Korting, U. Bock, et al., ATLA 36:161–187, 2008.

67. T. Hu, R. Bailey et al., Toxicol. Lett. 188(2):119–129, 2009.

68. S Lombardi Borgia, P. Schlupp et al., Eur J Pharm Biopharm. 68(2):380-9, 2008

69. G. Mun, M. Aardema et al., Mutat Res. 17, 673(2):92-9, 2009

70. Y. Park, J. Kim et at., Toxicology. 267(1-3):178-81, 2010.

71. A. Murray, E. Kisin et al.,Toxicology. 29;257(3):161-71, 2009.

72. I Horan, M. Clotworthy et al., J Ethnopharmacol. 89(1):81-90, 2003

73. ESAC Statement on the Application of the EpiDerm™ Human Skin Model for Skin Corrosivity Testing, March 2000, 3pp. Downloadable at: http:// ecvam.jrc.it, 2000.

74. L. Koeper, A.Schulz et al., Toxicology 242 (1-3):144-152, 2007.

75. M. Merkle, M. Kandsberger et al., ALTEX 16, 52,1999.

76. E. Heisler, J. Hoffmann et al., Immunobiology 206-209, 2002.

77. E. Heisler, J. Hoffmann et al., Toxicology Letters 144-1 S44, 2003

78. K. Mewes, R. Raus et al., Skin Pharmacol Physiol. 20(2):85-95, 2007

79. N. Zöller, S. Kippenberger et al., Toxicol. In Vitro. 22(3):747-59, 2008

80. M. Meloni, A. Farina et al., Photochem Photobiol Sci. 9(4):439-47, 2010

81. Ackermann K, Borgia SL et al. Skin Pharmacol Physiol. 23(2):105-12, 2010

82. C. Wiegand, N. Hewitt et al. Submitted for publication, 2012.

83. K. Reisinger, Personal communication.

84. B. De Wever B, A. Goldberg et al., ALTEX, 2012

85. Y. Poumay, F. Dupont et al., Arch. Dermatol. Res. 296:203-211, 2004.

86. Y. Poumay Y, A . Coquette, Arch. Dermatol. Res. 298:361-369, 2007.

87. A. Heymer, L. Schober et al., Presented at the DECHEMA Symposium, Zurich, Switzerland, 2012.

88. K. Mewes, Personal communication

89. S. Vankoningsloo, J. Piret et al., Nanotoxicology, 2009

90. B. Allen-Hoffmann, S. Schlosser, et al. J. Invest. Dermatol. 114(3):444-455

91. C. Rasmussen, A. Gibson, et al., Ann. Surg. 251(2):368-376, 2010.

92. J. Loertscher, C. Sattler et al., Toxicol. Appl. Pharmacol. 175(2):121-129, 2001

93. A. Gibson, M. Schurr et al., Tissue Eng. Part A 14(5):629-638, 2008

94. C. Rasmussen, A. Gibson et al., Ann. Surg. 251(2):368-376, 2010

95. M. Slavik, B. Allen-Hoffmann et al., BL, BMC Dev. Biol. 7:9 , 2007

96. J. Straseski, A. Gibson et al., Wound Repair Regen. 17(4):606-16, 2009

97. E. Gill, J. et al., Microsc Microanal. 16(2):117-31; 2010.

98. C. Rasmussen, K. Gratz et al., Tox In Vitro 7:2021-2029, 2010

99. C. Thomas-Virnig, J. Centanni et al., Molecular Therapy 17(3):562-9, 2009

100. C. Rasmussen, A. Gibson et al., Ann. Surg. 251(2):368-376, 2010

101. C. Rasmussen, Personal Communication

102. M. Niwa, K. Nagai et al., Biol Pharm Bull. 32(2):203-8, 2009.

103. M. Katoh, F. Hamajima et al., J Toxicol Sci. 34(3):327-34, 2009

104. M. Katoh, F. Hamajima et al., J Toxicol Sci. 35(3):411-7, 2010

105. H. Kojima T. Ando et al., Altern Lab Anim. 40(1):33-50, 2012

106. N. Morikawa, K. Morota et al., Altern. Animal Test. Experiment 9:1-10, 2002

107. K. Morota, N. Morikawa et al., Altern. Animal Test. Experiment 6:41-51, 1999

108. N. Morikawa, K. Morota et al., Altern. Animal Test. Experiment 11, 68-78, 2005

109. H. Kojima, T. Ando et al., AATEX 13(1):36-44, 2008

110. JACVAM, http://jacvam.jp/files/effort/01-001/01_001_05_en.pdf, 2008

Chapter 2

Realization and characterization of 3D_human dermis equivalent model

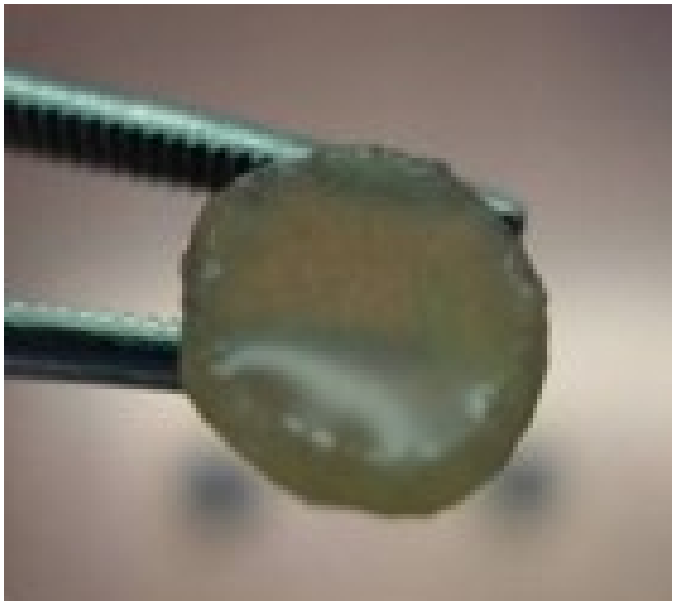

Introduction

The existing in vitro skin models reported in literature and described in the previous chapter are essentially based on cellularised fibrillar exogenous collagen.

Nevertheless, even if this model are widely used as in vitro dermal substitute they represent too simplified model to mimic the complex structure of dermis made up on cells embedded in a structured ECM composed by collagen, elastin and glycosomminoglycans. As consequence an exogenous bovine collagen can not mimic correctly such a complex structure and can not allow the recapitulation of pathway that in vivo plays a fundamental role in phenomena such as aging, photoaging or other events in which the structural proteins of ECM are involved.

The ECM is the non-cellular component present within all tissues and organs, and provides not only essential physical scaffolding for the cellular constituents but also initiates crucial biochemical and biomechanical cues that are required for tissue morphogenesis, differentiation and homeostasis. The importance of the ECM is vividly illustrated by the wide range of syndromes, which can be anything from minor to severe, that arise from genetic abnormalities in ECM proteins [1].The ECM is a highly dynamic structure that is constantly being remodeled, either enzymatically or non-enzymatically, and its molecular components are subjected to a myriad of post-translational modifications. Through these physical and biochemical characteristics the ECM generates the biochemical and mechanical properties of each organ, such as its tensile and compressive strength and elasticity, and also mediates protection by a buffering action that maintains extracellular homeostasis and water retention.

Formation of ECM is essential for processes like growth, wound healing, and photoaging etc. For example, an understanding of ECM structure

and composition also helps in comprehending the complex dynamics of tumor invasion and metastasis in cancer biology as metastasis often involves the destruction of extracellular matrix by enzymes such as serine proteases, threonine proteases, and matrix metalloproteinases.

In this perspective, we have developed a 3D-human dermis equivalent construct with properties similar to native dermis through an engineering approach defined modular or bottom-up approach [2-3].

One of the major challenges of bottom-up tissue engineering is to assemble modular tissues with specific micro architectures into macroscale biomimetic engineered tissues. Other challenge is to retain the microarchitecture and cellular behavior of modular tissues, while creating engineered tissues with robust mechanical properties.

We started from the realization of human dermis microtissue precursors (HD-μTPs) through the seeding of the cell on the microscaffold followed by a phase of aggregation of μTPs until the formation of a 3D-Human Dermis Equivalent model (called 3D_HDE).

This model represents a real innovation in tissue engineering and we have demonstrated that morphological, biochemical characteristics are very similar to native tissue.

MATERIALS AND METHODS

Microscaffold production

Preparation of porous gelatin microbeads

Gelatin porous microbeads (GPMs) have been prepared according to a modified double emulsion technique (O/W/O) [4]. Gelatin (type B Sigma Aldrich Chemical Company, Bloom 225, Mw=l 76654 Dalton) was dissolved into 10 ml of water containing TWEEN 85 (6% w/v) (Sigma Aldrich Chemical Company). The solution was kept at 60°C. Toluene containing SPAN 85 (3% w/v) (Sigma Aldrich Chemical Company) was continuously added to the aqueous gelatin solution (8 % w/v) to obtain primary oil in water emulsion. The added toluene formed droplets in the gelatine solution until saturation. Beads of gelatine containing droplets of toluene were produced through the addition of excess toluene (30 ml). The overload of toluene allowed the obtaining of a double emulsion (O/W/O). After cooling below 5°C, 20 ml of ethanol was added to extract toluene and stabilize GPMs. The resulting microspheres were filtered and washed with acetone and then dried at room temperature. Microspheres were separated selectively by using commercial sieves (Sieves IG/3-EXP, Retsch, Germany). GPMs with 75-150 μm size range were recovered and further processed. Finally the microbeads morphology has been examined by means of Scanning Electron Microscopy (SEM).

Crosslinking of GPM

GPMs have been stabilized by means of chemical treatment with glyceraldehyde (GAL), in order to make them stable in aqueous environment at body temperature. In particular, GPMs were dispersed into acetone/water solution containing 5% of GAL and mixed at 4°C for 24 h. Then microspheres were filtered and washed with acetone and dried at room temperature.

HD-µTP precursors characterization

Human dermal fibroblasts (neonatal HDF ,Cell Applications, Inc, UK) were sub-cultured onto 150 mm Petri dishes in culture medium (Eagle's BSS Minimum Essential Medium containing 20% fetal bovine serum, 100 mg/mL L-glutamine,100 U/mL penicillin/streptomycin, and 0,1 mM Non Essential Amino Acids). Cells were maintained at 37°C in humidified atmosphere containing 5% CO_2. HDF of passages 6-12 and GPM crosslinked at 5% (5% GPM) have been used for all experiments. Before using dry GPM were sterilized by absolute ethanol sub-immersion for 24h. Successively to remove completely the ethanol several washings in calcium-free and magnesium-free phosphate-buffered saline (PBS) were performed. Before cell seeding PBS was removed and replaced with the culture medium. HD-µTPs cultivation was initiated by inoculating HDF at 10 cells bead^{-1}. The culture suspension was stirred intermittently at 30 rpm (5 min stirring and 30 min static incubation) for the first 6h post-inoculation for cell adhesion, and then continuously agitated at 30 rpm. The growth medium was replenished on the first day and every 2 days until the end of experiments (9 days in total). From the day 4th 50µg/ml of ascorbic acid was added. HD-µTP samples were taken for assay at day 1, 3, 6 and 9. The rate of disappearance of free cells from inoculated microcarrier cultures was determined as an indication of cell attachment to microcarriers. During the intermittent stirring phase culture sample (500 µl) was taken each hour and allowed to settle for 1 min in an Eppendorf tube. The microcarrier-free supernatant was introduced into a hemocytometer for cell counting. After counting the free cells in the medium with a hemocytometer, the number of cells adhering to microbeads (cell/microbead ratio) was evaluated. About 1ml aliquots were collected at day 1,3,6 and 9 from spinner culture for the cell adhesion assay on the microcarriers. Briefly, 300 µl of the same aliquots was transferred to a cell culture dish (w/2 mm grid Nunc) for microcarrier

counting, experiments were performed in triplicate. After that the microcarriers suspension was placed in the 1,5ml eppendorf tube, gently washed twice with PBS, and then treated with trypsin solution to allow cell harvesting. Finally, the detached cells were counted using a hemocytometer.

Scanning electron microscopy (SEM)

SEM was performed to analyze the morphology of microbeads and of µTP precursors. The microbeads didn't need any dehydratation process so they were mounted onto metal stubs using double-sided adhesive tape and then gold-coated using a sputter coater at 15 mA for 20 min. Coated samples were then examined by scanning electron microscopy (SEM) (Leica S400). Instead the µTP precursors needed to be dehydratated, the dehydratation was carried out by gradually decreasing the water concentration and increasing the ethanol concentration (75%, 85%, 95% and 100%, and 100% again, each step 20 min at room temperature). Finally the samples were treated following the procedure explained above for dried samples.

3D human dermis equivalent model

HD-µTP molding

As previously described [5] HD-µTPs suspension was transferred from the spinner flask to a 50 ml Falcon centrifuge tube and, after settling, transferred by pipetting into the maturation chamber to allow their molding in disc-shaped construct (1 mm in thickness, 5 mm in diameter). During the filling procedure, the maturation chamber was accommodated on a device connected with a vacuum pump to make the process faster and to assure that any bubble was in the maturation space.

This chamber has a "sandwich-like" structure, the center of which there is a silicon mold with four blank spaces, where takes place the assembly of µTPs. The silicon mold is bounded both on the lower side both on the

upper one of two rigid grids of stainless steel characterized by a porous network for retaining µTPs and for allow an efficient and homogeneous supply of nutrients. Two rings of polytetrafluoroethylene (PTFE) are placed on the racks on both sides of the chamber and held together by four screws which ensure the closing of the system (fig.1) [6,7].

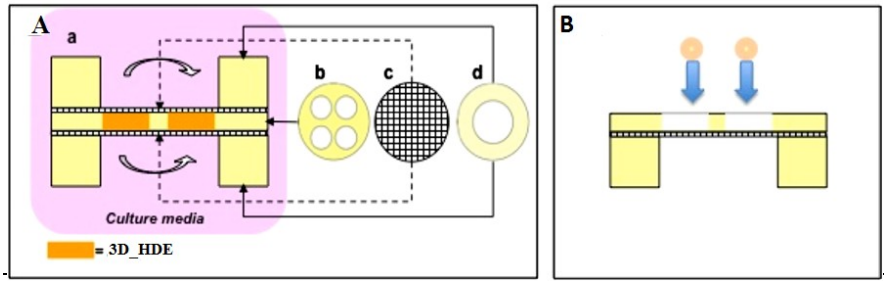

Figure 1: Assembling maturation chamber(A), showing the configuration of the assembling chamber during the assembling process of µ-TPs (a), the silicon mould with four empty spaces (b), the rigid mesh with 18 µm pore size (c) and the PTFE ring (B); µ-TPs loading (C).

Maturation of 3D-HDE was carried out until 2 weeks in dynamic conditions by placing the chamberon the bottom of a spinner flask operated at 60 rpm at 37 °C, 5% CO_2 and humidity 90%. The medium was changed every 2 days and at each medium change ascorbic acid was added at a concentration of 50 µg/ml.

Characterization of 3D_HDE model

ECM morphology and composition

The samples were fixed in a solution of 4% paraformaldehyde for 30 min at room temperature, rinsed twice with PBS buffer solution and soaked into a sucrose water solution (2M). After 24 hours samples were included in Tissue Tek (Killik) in a suitable mold (Peel-A, Ted Pella INC) and submerged in liquid nitrogen vapors for 1 min and then stored at -80 °C. All samples were cut in slices 5 µm in thickness by using

criomicrotome (Leica CM 1850). The cut was oriented so as to view the cross section of the samples.

ECM composition and morphology along the 3D_HDE thickness were assessed by performing histological and immunofluorescence analysis on transverse sections of sample.

Histological analyses

7µm transverse sections of samples were stained using hematoxylin-eosin (Bio Optica) solutions, Masson tricromic (Sigma Aldrich) and Picro Sirius Red (PSR) (Sigma Aldrich) following standard procedure and analyzed by an optical microscope (BX53; Olympus).

Polarized light images of samples stained with PSR alone were acquired with an inverted microscope (BX53; Olympus) with a digital camera (Olympus DP 21). A linear polarizer was placed between the light source and the specimen, while the analyzer was installed in the light path between the specimen and the camera. It is known that the color of collagen fibers stained with picrosirius red and viewed with polarized light depends upon fiber thickness; as fiber thickness increases, the color changes from green to red [8,9].

Immunofluorescences analyses

For immunofluorescences analyses (IF), the slices were permeabilized with 0.01% Tritox X-100 in PBS/BSA 3% for 1 hour at room temperature. Subsequently, the slices were incubated for 3 hours at room temperature with primary antibodies followed by incubation of appropriate secondary antibody for 2 hours at room temperature. Moreover Hyaluronic acid and fibronectina were performed respectively as dermal markers: anti-Hyaluronic acid polyclonal antibody (Abcam), anti-fibronectin monoclonal antibody (Sigma). Every antibody monoclonal were produced in mouse and the polyclonal antibody were produced in rabbit. The nuclear stain

was Sytox Green (Invitrogen) and Dapi staining. The secondary antibodies that we used were: 546 Rabbit Anti-Sheep IgG H&L (Abcam), Alexa Fluor 546 goat anti-mouse IgG (H+L) (life tecnologies). All secondary antibodies was diluted 1:500 in PBS/BSA 3%.

Collagen structure by second harmonic generation imaging

Second harmonic generation _SHG_ imaging has recently emerged as a noninvasive tool for high-resolution imaging of fibrillar type I collagen in tissues. Simultaneous interaction of two near-infrared _NIR_ photons with non centrosymmetric structures can result in emission of a single photon at exactly half the wavelength of the excitation light. In particular, collagen type I produces a very robust SHG signal with a nonlinear excitation wavelength between 700 and 1064 nm, allowing a window of detection from 350 to 532 nm.

Because individual collagen fibrils are the source of the SHG signal, this method has the potential to spatially resolve collagen organization at the submicrometer level and provide information regarding physiological changes in collagen structure that correlate with tissue function.

The samples for second harmonic generation imaging were prepared as previously described, but a slice thickness of 50 µm was choose. Before imaging, samples were unfrozen and closed with a microscope cover slide together with some droplets of glycerol-water solution in order to maintain the natural tissue osmolarity.

SHG imaging in our samples were performed using a Confocal Leica TCS SP5 II femtosecond laser scanning system (Leica), coupled to a tunable compact mode-locked titanium:sapphire laser (Chamaleon Compact OPO-Vis ,Coherent).The samples were observed by using λ_{ex} = 840nm (two photons) and λ_{em}=415-425nm. The SHG images, having a size of 200µm x 200µm, were acquired with a resolution of 12bit, 1024x1024 pixel by using a 40X N.A. 1.25 objective.

RESULTS AND DISCUSSIONS

Microscaffold characterization

Gelatin porous microbeads (GPMs) have been prepared according to a modified double emulsion technique (O/W/O) and have been separated selectively using a sievers in the range of 75-150 µm size. Afterwards the GPMs were stabilized with a chemical treatment with glyceraldehydes in order to make stable in aqueous environment and finally have been characterized by scanning electron microscopy (SEM).

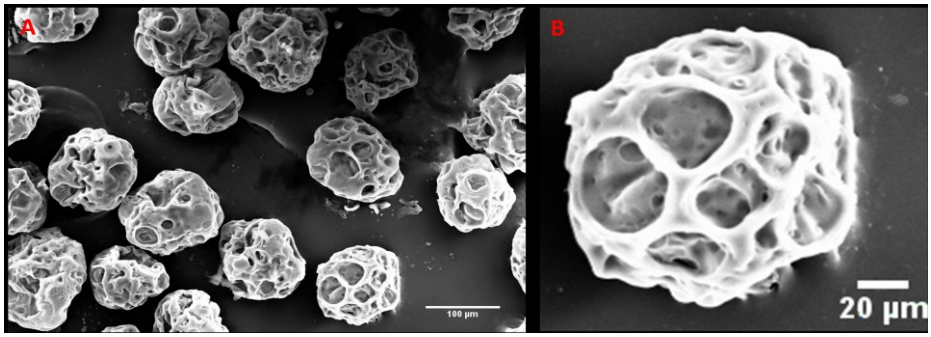

Figure 2: GPMs morphology: SEM micrographs of 5% GPM (A) and zoom of single GMP (B).

The SEM images (fig 2 A,B) showed the GPMs morphology in which are clearly visible a good sphericity and a high porosity.

The images show an overview of the GMPs (fig.2- A) as well as an image of a single GMP(fig2-B) in which are visible interconnected pores of about 20 µm in diameter, uniformly distributed on the surface and in the bulk of GPMs.

Characterization of HD-µTP precursors

HD-µTPs cultivation was initiated by inoculating HDF at 10 cell to bead, corresponding to 10^5cell*ml^{-1} and 2mg*ml^{-1} of microbeads in the spinner flask(fig 3).

The culture suspension was stirred intermittently at 30 rpm for the first

6h post inoculation in order to promote the adhesion of the cell to the beads [10].

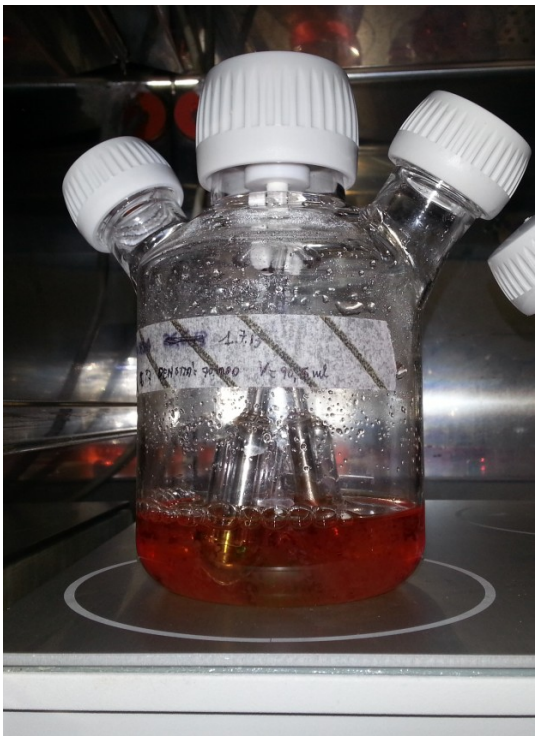

Figure 3 : Spinner flasks bioreactor incubated

The disappearance of free cells from the inoculated spinner cultures was considered to indicate the attachment of cells to the microcarriers. In the figure 4-a is reported the seeding efficiency calculated as $[(C_0-C_t)*100]/C_0$ where C_0 is the concentration of the HDF at the inoculum time and C_t the concentration of the HDF in the culture medium at each hour of the intermittent seeding phase of spinner culture. It was possible to observe that seeding efficiency was ≈95%.

Moreover, the cell adhesion as well as cell proliferation during the spinner culture were evaluated at day 1, 3, 6 and 9. In the figure 4-b was reported the cells/microbead ratio increasing up to ≈ 100 cell*bead^{-1}.

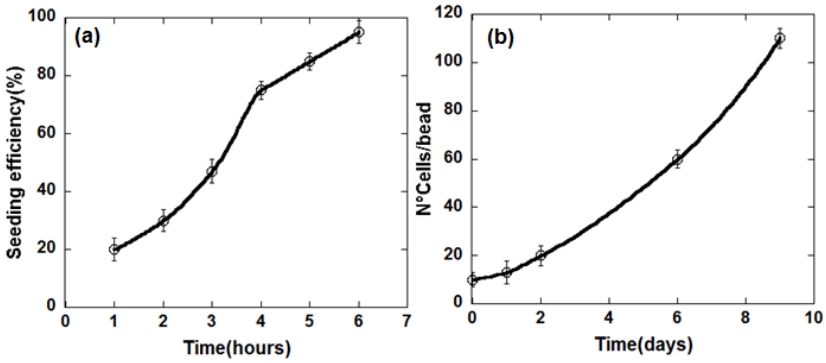

Figure 4 : Cell seeding (a) and cell proliferation (b) of HDF on GPMs.

Sem images show the morphology of µTP precursors at 9 days of spinner culture (fig 5a-b) in which it is clearly visible the dense network of collagen which is formed both around microbeads that between the microbeads themselves.

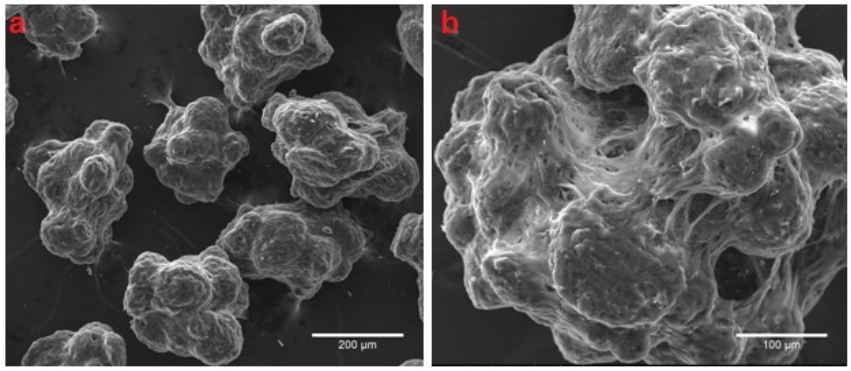

Figure 5: sem images of µTP precursor at 9 days of spinner culture. Scale bar 200µm (a); 100 µm (b)

3D human dermis equivalent model

HD-µTP molding

The HD-µTC were transferred from the spinner flask in a maturation chamber to allow their molding in a disc-shaped construct (1 mm in thickness, 5 mm in diameter) (fig. 6) inserted in a dynamic environment

allowing tangential flow that guarantee optimal nutrient supply and waste removal through the maturation space during the culture time.

The culture time has been explored at 2 weeks.

At 2 weeks of culture it was evident by the images 6 B-C that 5% 3D_HDE retained the disc shape of the mold, are compact and can be handled without any damage.

The optimization of the filling process has allowed to obtain homogeneous and compact biohybrid that retains the shape and size of the maturation chamber even after the removal of the same from the chamber. The biohybrid removed from the mold disc-shaped, has a completely smooth surface, remains intact and shows a certain elasticity and firmness.

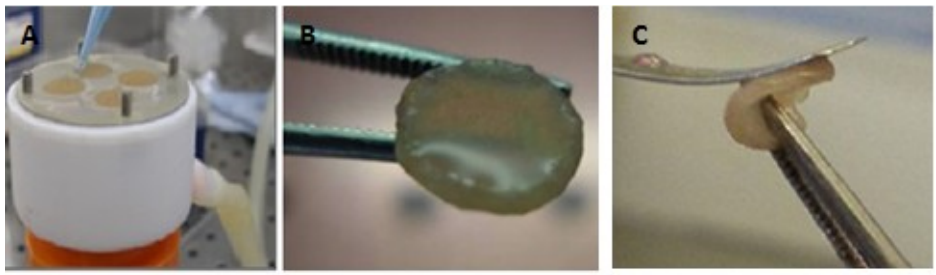

Figure 6 : HD-µTC molding(A); Two pictures(A,B) of the 3D_HDE obtained. As you can see the biohybrid is compact and flexible, the surface is completely smooth.

ECM morphology and composition:

Histological and immunofluorescences analyses

ECM composition and morphology along the 3D_HDE thickness were assessed by performing histological and immunofluorescences analyses.

The figure 7 shows histological images, respectively, of hematoxylin-eosin; picrosirius red and masson trichrome staining concerning 3D_HDE at 2 weeks of maturation.

In the figure 7-A it is possible to observe that the extra-cellular matrix is homogeneous in its composition along the thickness of the sample and

the fibroblasts are completely immerse in collagen matrix and the elongated nuclear morphology underlines the good condition of the cells in their own extracellular matrix.

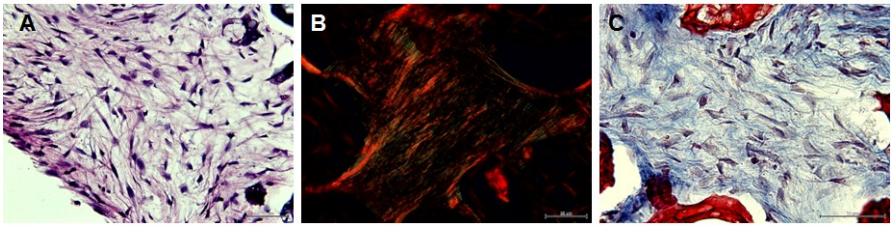

Figure 7: Hystological image of 3D_HDE: hematoxylin-eosin (A); picrosirius red (B) and masson tricromic(C) staining. Scale bar 50µm.

The figure 7-B show Picrosirius red staining that allows to discriminate the collagen fibers, from mature fibers or type I to immature fibers or type III by the use of a polarized light microscope.

The red signal corresponds to thick mature collagen fibers while the green signal corresponds to thin immature collagen fibers.

Finally, masson tricromic histological staining are reported in the image 7-C. It is possible to see that collagen (in blue) is uniformly present along the whole thickness of sample.

In figure 8 are presented some markers of the extracellular matrix both for in vitro our model and for native human dermis. All immunofluorescence analysis were performed on frozen transverse section 7µm thick and as nuclear dye was chosen dapi (fig 8 A, B) and sytox green (fig C,D).

In detail, the image A and B shows fibronectin in red and dapi as nuclear staining, while in the image C and D is shown hyaluronic acid (in red) and sytox green for cell dye. Fibronectin is the second most abundant protein in ECM, where it is organized into a fibrillar network and in 3D_HDE (fig 8B) the fibronectin signal is more similar to native tissue(fig 8A).

Hyaluronic acid is non collagenous component of ECM and, in the extracellular space, confers upon tissues the ability to resist compression

by providing a counteracting turgor (swelling) force by absorbing significant amounts of water. Immunofluorescence staining demonstrated, in the 3D-HDE, the presence of hyaluronic acid (fig 8D) around cells in ECM and this is concorde with signal offered by native tissue (fib 8C).

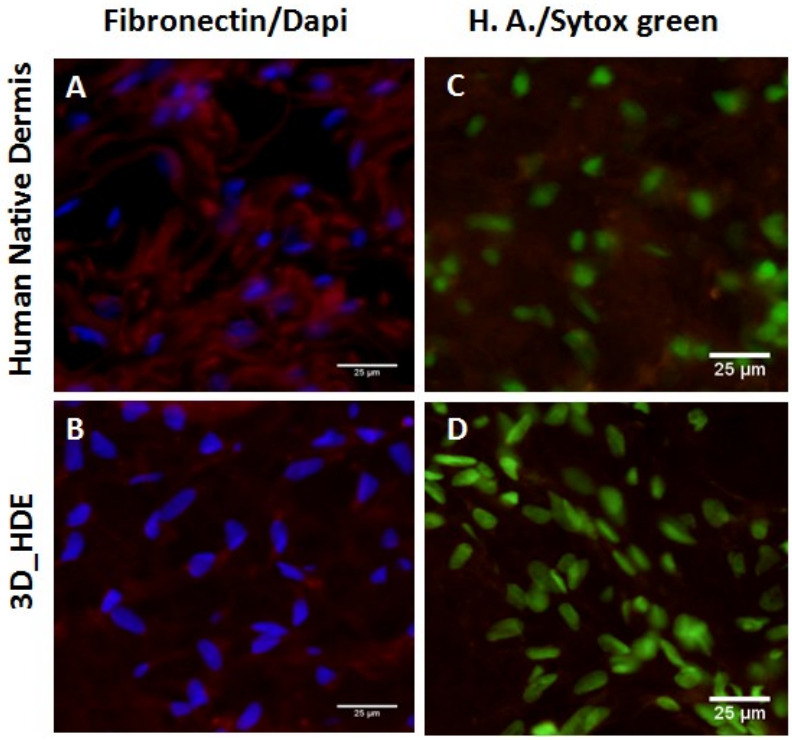

Figure 8:Immunofluorescence images of Human native dermis and 3D_HDE. Frozen section were immunostained for fibronectin(red)(A-B) and dapi as nuclear stain, hyaluronic acid (C-D) and sytox green as nuclear stain. Scale bar 25µm.

Collagen structure by SHG imaging

The collagen fibrils structure was observed by using MPM that allow to visualize unstained collagen structure by exploiting SHG.

The figure 9 shows the SHG signal (gray) and cells (green) of human native dermis (fig. 9A) and of 3D_HDE with different magnifications (fig.9 B-D). In our model is visible the presence of collagen around the cells and the presence of collagen secreted from human fibroblasts

suggested that the cells not only proliferated but also work correctly like natural dermal fibroblasts by secreting collagen.

Besides, as can be seen in the images 9 B, C, D, the collagen matrix of 3D_HDE is a denser and more organized fine structure with long fibrils similar to native dermis.

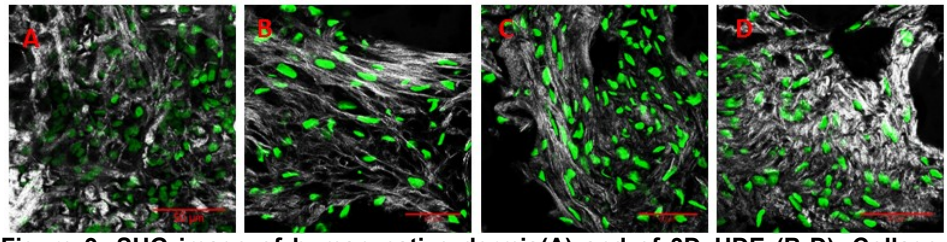

Figure 9: SHG image of human native dermis(A) and of 3D_HDE (B-D). Collagen matrix in gray and cells in green. Scale bar 50µm.

Conclusion

In conclusion, we have demonstrated that two-step approach based on μTP precursor production and their further association is a viable strategy to build-up human dermal tissue equivalent in vitro composed of all endogenous ECM components. We have characterized this tissue, showing , that from a morphological and biochemically point of view, is similar to the native dermis in terms of cellular and extracellular components**.** This in vitro model represents a real innovation in tissue engineering and it can be used in to study all the phenomena involved in the dermis diseases.

.

REFERENCES

1. Jarvelainen, H., Extracellular matrix molecules: potential targets in pharmacotherapy, Pharmacol (2009)

2. Kelm JM et al. Design of custom-shaped vascularized tissues using microtissue spheroids as minimal building units. Tissue Eng12(8):2151–60 (2006);

3. McGuigan AP, Sefton MV. Vascularized organoid engineered by modular assembly enables blood perfusion. Proc Natl Acad Sci USA 103(31):11461–6(2006);

4. Nilsson K, Buzsaky F, Growth of anchorage-dependent cells on macroporous microcarriers. Nature Biotech; 4:989-990(1986)

5. Urciuolo F, Imparato G,et al. Effect of Process Conditions on the Growth of Three-Dimensional Dermal-Equivalent Tissue Obtained by Microtissue Precursor Assembly. Tissue Eng.;17:155-64 (2011).

6. Palmiero, C., "Engineered dermal equivalent tissue in vitro by assembly of microtissue precursors", Acta Biomaterialia 6 (7), 2548-2553, (2010).

7. Urciuolo F. "Novel strategies to engineering biological tissue in vitro", Methods Mol Biol 811, 223-244, (2012).

8. Rich L, Whittaker P. Collagen and picrosirius red staining: a polarized light assessment of fibrillar hue and spatial distribution. Braz. J. morphol. Sci.; 22-97-104 (2005).

9. Nadkarni SK et al; Measurement of Collagen and Smooth Muscle Cell content in Atherosclerotic Plaques Using Polarization-Sensitive Optical coherence Tomography. Journal of the American College of Cardiology 49:1475-1481 (2007).

10. Ng YC, Berry JM. Optimization of physical parameters for cell attachment and growth on macroporous microcarriers. Biotech and bioeng, 50:627-35 (1996)

Chapter 3

Endogenous human dermis as a novel in vitro tool to quantify UVA-induced ECM alterations and efficacy of photoprotectants

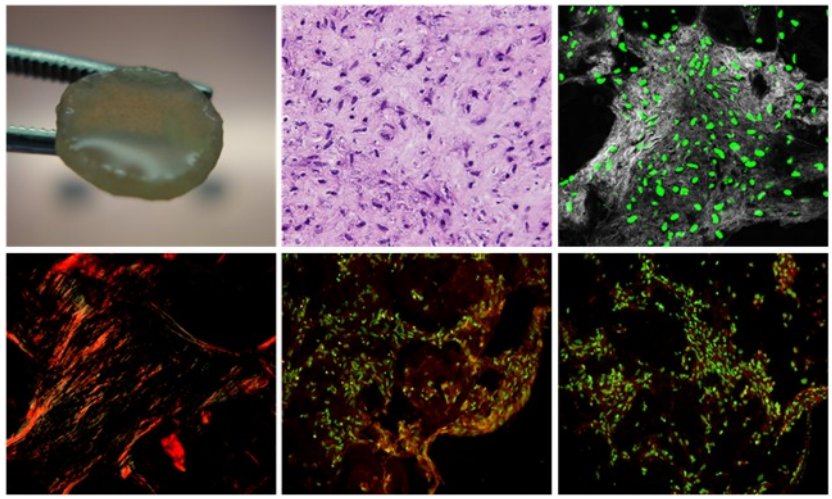

Introduction

In this chapter we validated the human dermis equivalent model, as an in vitro model to study collagen network re-arrangement and photo-protectans efficacy under simulated solar exposure.

Damage to the collagenous extracellular matrix (ECM) that comprises the skin connective tissue is a characteristic feature of chronically sun exposed human skin, and is thought to underlie the coarse, rough, wrinkled appearance that is the hallmark of photoaged skin [1,2].

Photoaging is mainly caused by UVA radiation, which due to its high penetration properties, can reach deeper parts of the skin and affects the dermal compartment [3]. *In vivo* studies have given clear evidence that UVA exposure induced dermal structure deterioration causing clinical changes observed in photoaged skin. However experimental chronic UV exposure are difficult to perform in humans and animals for ethical reasons as well as significant costs [4]. On the other hand, neither two-dimensional conventional cell cultures nor three-dimensional cell cultures in exogenous scaffold reproduce physiological conditions as well as structural and biological aspects of native dermis. Indeed a biological tissue is not a combination of cells within a bundle of inert macromolecules, but it is rather an intricate complex of cell and cell-synthesized matrix that constitute a unicum element regulated by a multifaceted homeostatic equilibrium. Cells are regulated and controlled by the ECM composition and structure, which, in turn, are synthesized, assembled and remodeled by cells. Tissue pathology or dysfunction even when arisen from cellular components affects the extracellular space and vice versa [5-7].

It is widely recognized that alteration of the dermal ECM microenvironment due to UV exposure have significant consequences on the fibroblast function which produce more MMP and less collagen modifying the tissue homeostasis [8]. The existing 3D model are able to

recapitulate the cell response occurring after UVA irradiations but, at the best of our knowledge no *in vitro* models can analyzed the alterations, in the structure, composition and architecture of dermal ECM. In this study, by instructing human dermal fibroblast in synthesizing and assembling their own ECM, we realized a dermis like tissue rich in endogenous ECM, recapitulating the complex homeostatic equilibrium and dynamical reciprocity between the cellular and extracellular space. We hypothesize that due to its endogenous nature our model is able to mimic both the physiological and pathological status of a native tissue such as photoaging. So we performed UVA irradiation and quantitatively linking photo-aging process with ECM alteration by multi-photon microscopy (MPM), histological and immunofluorescence analysis. We investigated the feasibility of using our endogenous human dermal equivalent (HDE) to confirm the well-known photoprotective effect of retinoic acid on UVA induced damages as well as to determine the effect of Dolichos biflorus cell culture extract. The latter was previously demonstrated acting on multiple fronts in preventing and protecting skin cells from photodamage, thanks to the presence of important flavonoids in its composition [9]. Our data demonstrated that HDE allows to deeply investigate the phenomena involved in dermis photoaging and correlate the damage at cellular and extracellular level with collagenous coarsening and ECM organization.

MATERIALS AND METHODS

Human dermis equivalent production

The realization of endogenous HDE has been performed by means of a previously reported bottom-up tissue engineering strategy (see chapter 2). Briefly, Human dermal fibroblasts were sub-cultured into 150 mm Petri dishes in culture medium (Eagle's BSS Minimum Essential Medium containing 20% fetal bovine serum, 100mg/mL L-glutamine, 100 U/mL

penicillin/streptomycin, and 0,1 mM Non Essential Amino Acids) and maintained at 37 °C, 5% CO_2 and humidity 90%. Dermal microtissue (HD-μTP) were produced by seeding HDF of passages 6-12 on gelatin porous microcarriers, in a spinner flask for 9 days and then transferred into the maturation chamber to allow their molding in disc-shaped tissue-construct such as HDE (1 mm in thickness, 5 mm in diameter) as previously described. Maturation of HDE was carried out until 2 weeks in dynamic conditions by placing the chamber on the bottom of a spinner flask operated at 60 rpm at 37 °C, 5% CO_2 and humidity 90%. The medium was changed every 2 days and at each medium change ascorbic acid was added at a concentration of 50 μg ml^{-1}. As control an exogenous human dermis equivalent was also produced by mixing human dermal fibroblasts and collagen type I. In particular, appropriate volume of bovine type I collagen (Sigma Aldrich)at concentration of 3 mg ml^{-1} was neutralized by dropwise addition of 0.1 NaOH and immediately mixed with $3x10^4$ HDF (passage 5) to yield a final concentration of 2.4 mg/ml. The solution (300 μl per well of a 24-well transwell plate) was placed in an incubator at 37°C for 45 minutes to allow the polymerization of the collagen. Throughout the manuscript we referred to this model such as fibroblast-populated collagen.

UVA source and irradiation

Samples were exposed to UVA radiations by using a UVA lamp (UVP lamp 3UV 38, cod. 95035, TERMO SCENTIFIC, WATT 3X8) in order to simulate solar exposure. The samples (both 3D-HDE and fibroblast-populated collagen) were accommodated in multiwell and irradiated for 15 minutes at final power of 20 Joule/cm^2. The UVA lamp was mounted on a stable support allowing an exposure distance of 2 cm from the sample surface. Samples sterility was guaranteed by performing irradiation under biological hood.

Sunscreen formulation and evaluation of photoprotection

Dolichos biflorus cell culture extract was previously characterized for its properties to protect skin cell from UV induced damage[9-10] . For our experiments a formulation of Dolichos extract at 0.01% was used. As positive control retinoic acid (1 μM) was used. Treatments with sunscreen were performed by adding Dolichos or retinoic acid in the culture medium 4 hours before UVA exposure. To avoid the formation of phototoxic products, immediately before performing UVA irradiation, culture medium was withdrawn and substituted with fresh PBS solution. Samples were divided into four groups:

- Control (not UVA exposed and sunscreen not treated)
- UVA (UVA exposed and sunscreen not treated)
- UVA Dol (UVA exposed and Dolichos treated)
- UVA Ret (UVA exposed and retinoic acid treated)

As control for each group, fibroblast-populated collagen was used. At the end of UVA exposures PBS solution was removed and fresh medium with or without sunscreens was added. The UVA-induced damage and sunscreen protecting effects were evaluated 6 and 72 hours after UVA exposure for all samples.

Histological analyses

All samples were fixed in 4% paraformaldehyde for 30 min at room temperature, washed in PBS and soaked into a sucrose water solution (2 M). After 24 hours samples were included in Tissue Tek (Killik) in a suitable mold (Peel-A, Ted Pella INC) and submerged in liquid nitrogen vapors for 1 min and then stored at -80 °C. All samples were cut in slices 7 μm in thickness by using criomicrotome (Leica CM 1850).

Hematoxylin-Eosin (H/E) staining was performed in order to evaluate ECM morphology and stained samples were analyzed by an optical microscope (BX53; Olympus). The cell nuclei were stained by SYTOX®

Green (Invitrogen, Life Technologies). The samples were observed by using the following filter λ_{ex}=504 nm and λ_{em}=523 nm. Moreover, mature and immature collagen morphology was assessed by staining 7µm transverse sample sections with Picro Sirius Red (PSR) (Sigma Aldrich). Then stained sample were observed by using an inverted microscope (BX53; Olympus) with a digital camera (Olympus DP 21). A linear polarizer was placed between the light source and the specimen, while the analyzer was installed in the light path between the specimen and the camera.

The color of collagen fibers stained with Picro Sirius Red and viewed with polarized light depends upon fiber thickness; as fiber thickness increases, the color changes from green to red.

For quantitative analyses Picro Sirius red images were analyzed by using image J® software. In order to quantitatively determine the proportion of mature (red) and immature (green) collagen fibers, we resolved each image into its hue, saturation and brightness (HSB) components by using Image J software "color threshold" function. Only the hue component was retained and a histogram of hue frequency was obtained from the resolved 8-bit hue images, which contain 256 colors. We used the following hue definitions; red 0-51, green 52-120[5,11]. The analysis was performed on 20 Picro Sirius Red stained sections of sample. About 5 region of interests (ROIs) were examined for each section.

Immunofluorescences analyses

For immunofluorescences analyses, the 7 µm thick slices were permeabilized with 0.01% Tritox X-100 in PBS/BSA 3% for 1 hour at room temperature. Subsequently, the slices were incubated for 3 hours at room temperature with primary antibodies followed by incubation of appropriate secondary antibody for 2 hours at room temperature. The

primary monoclonal antibodies used in this study include: anti-MMP1 polyclonal antibody red (diluted 1:200, Abcam), anti-MMP9 monoclonal antibody red (diluted 1:200 Abcam) and Anti-Hyaluronic acid polyclonal (diluted 1:50, Abcam). The secondary antibodies used were respectively: Alexa Fluor (Life Technologies) 568 goat anti-rabbit, Alexa fluor (Life Techologies,) 568 goat anti-mouse and 546 Rabbit Anti-Sheep IgG H&L (Abcam), all secondary antibodies was diluted 1:500 in PBS/BSA 3%. The samples were investigated by using optical microscope (BX53; Olympus). To quantitatively analyze MMPs and HA in each samples, images were processed by using image J® software and the signal was normalized to the cell number. Cells were counted by using the software function “analyzes particles”.

Second Harmonic generation imaging and GLCM texture analysis

For SHG imaging samples slice 50 μm thick were prepared. Before imaging, samples were unfrozen and closed with a microscope cover slide together with some droplets of glycerol-water solution in order to maintain the natural tissue osmolarity. Samples were investigated by confocal microscopy (TCS SP5 II Leica) combined with a MPM where the NIR femtosecond laser beam was derived from a tunable compact mode-locked titanium: sapphire laser (Chamaleon Compact OPO-Vis, Coherent).

Two-photon excited fluorescence was used to induce second harmonic generation (SHG) and obtain high-resolution images of unstained collagen structures. The samples were observed by using λ_{ex} = 840 nm (two photons) and λ_{em}=415-425 nm. The SHG images, having a size of 200 μm x 200 μm, were acquired with a resolution of 12 bit, 1024x1024 pixel by using a 40X N.A. 1.25 objective.

To quantitatively assess the collagen-related changes, we performed gray-level co-occurrence matrices (GLCM) texture analysis by using

ImageJ plug-in “Texture” on SHG images [12].

A running neighbor index allowed calculation of a GLCM matrix per neighbor index per SHG image. In detail, we evaluated correlation feature and if the correlation falls off sharply with pixel distance, the collagen matrix presents distinct, linear fibrils; if it remains elevated as pixel distance is increased, the collagen matrix has less defined fibrillar structure. In this work, we calculated the correlation curve for distances ranging from 1 to 200 pixels (corresponding to 1-40 μm) in the horizontal and vertical direction of each optical section that cover a length of interest of 40 μm. In such spatial windows the distance at which the correlation function fall off represents the correlation length of the texture. In particular Correlation curve was calculated versus neighbor index and correlation length was obtained by fitting data with an exponential low [12,13]

Statistical analyses

Data is expressed as mean ± SD. Differences between groups were determined using a nonparametric method, Kruskal-Wallis. Significance between groups was established for $p < 0.05$

RESULTS AND DISCUSSION

Micro and macroscopic morphology of endogenous HDE

To fabricate endogenous HDE, dermal microtissue(HD-μTP) were molded in a maturation chamber inserted in a dynamic environment allowing tangential flow that guarantees optimal nutrient supply and waste removal through the maturation space during the culture time.

As reported in the Figure 1a, HDE obtained after 2 weeks of culture retained the disc shape of the mold, it was compact and could be handled without any damage. Histological analyses with Hematoxylin-Eosin shows that fibroblasts retained the typical cytoskeletal morphology and are embedded in abundant endogenous ECM (fig. 1b). Moreover, images obtained at MPM show cells (green) embedded in the their own collagen network (grey) visualized by means of SHG (fig. 1c). The SHG signal was strong indicating a massive collagen fibers deposition and organized collagen bundles.

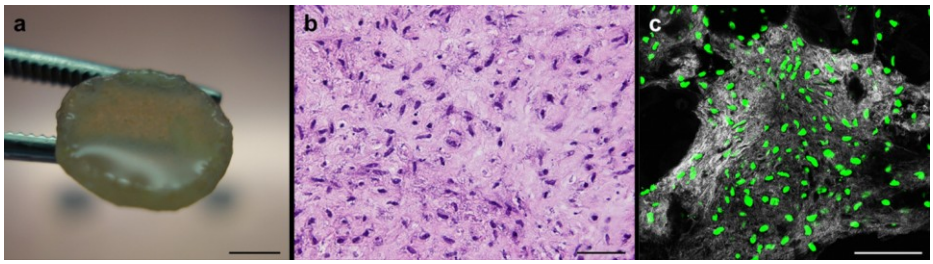

Figure 1: Macroscopic view of 3D_HDE model after 2 weeks of culture(a) scale bar 3mm; H/E staining (b) of 3D_HDE scale bar 50 μm; SHG signal and cells(green) , collagen network(gray), scale bar 50 μm

MMPs response in photo-exposed and photo-protected samples

Immunofluorescence analyses were performed in order to evaluate the expression of two classes of MMPs involved in photoaging process, such as MMP1 and MMP9. The image in Figure 2 shows MMP1 (fig. 2a-d) and MMP9 (fig.2e-h), 72 hours after UVA irradiation, in details the red signal indicates MMPs while the green one indicates the cells stained with Sytox green.

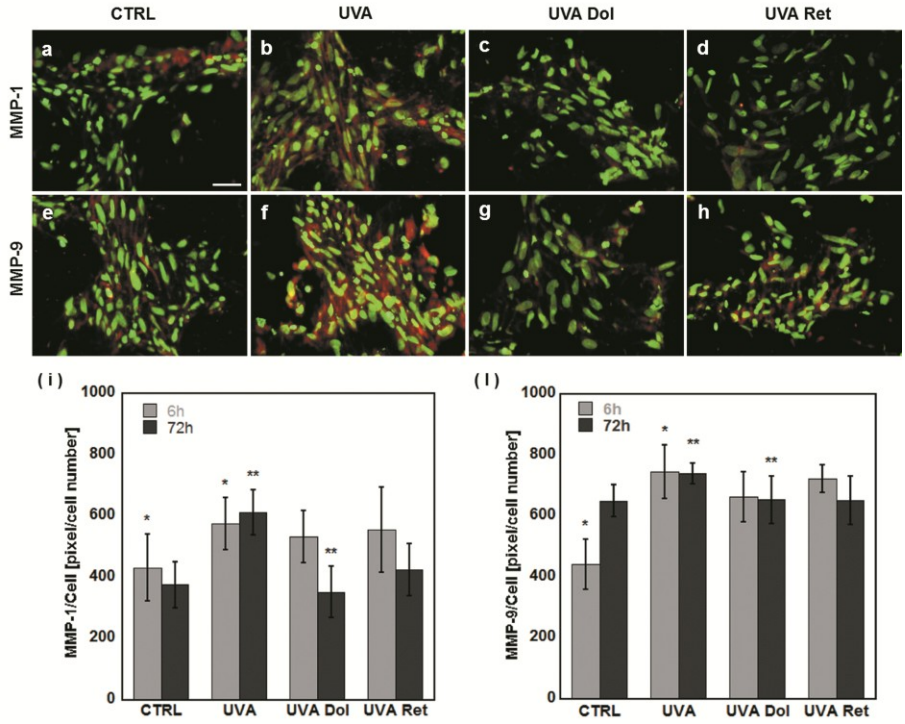

Figure 2: : Immunofluorescence analysis of 3D_HDE: Expression of MMP-1 (red) and SYTOX® Green (green) (a - d); Expression of MMP-9 (red) and Sytox (green) (e- h); quantitative analysis of MMP1/Cell(i) and MMP9/Cell (l) at 6 and 72 hours after UVA exposure. Scale bar 25 µm.

Quantitative investigations of immunofluorescence images show that MMP1 (fig.2i) and MMP9 (fig. 2l) per cells in HDE irradiated with UVA but not treated with sunscreen (UVA-HDE) increased respectively 1.33 and 1.68 time compared to the control sample 6 hours after UVA irradiation and 1.62 and 1.13 time 72 hours after UVA irradiation. Our

results confirmed the photo-protectants actions of Dolichos and retinoic acid in decreasing the MMPs production only at the second time points. Indeed at 72 hours the value of MMPs of photo-protected samples is pushed down to the values of the control. Immunofluorescence for MMPs performed on fibroblast-populated collagen confirmed an over-production in irradiated sample and a down regulation in photo-protected sample at both time points (fig 3).

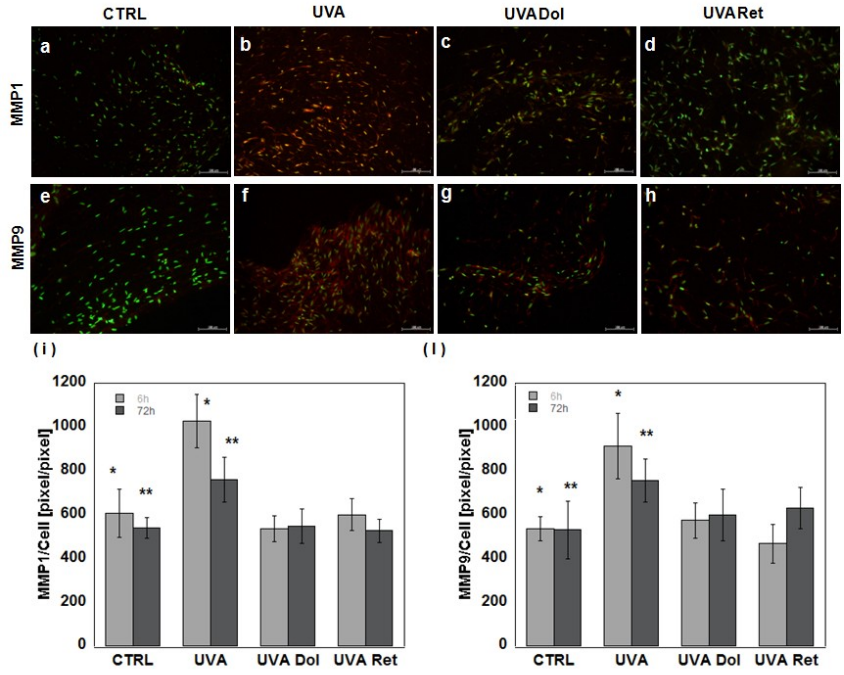

Figure 3: Immunofluorescence analysis of fibroblast-populated collagen. Expression of MMP-1 (red) and SYTOX®Green (green) (a-d); Expression of MMP-9(red) and Sytox (green) (e-h); quantitative analysis of MMP1/Cell(i) and MMP9/Cell (l) at 6 and 72 hours after UVA exposure. Scale bar 100µm.

Collagenous and non-collagenous dermal matrix in photo-exposed and photo-protected samples

Both collagenous and non-collagenous components of endogenous ECM have been investigated in order to evaluate the effects due to UVA irradiation and the anti-aging action of photoprotective. Mature and

immature endogenous collagen in HDE, have been investigated by means of Picro Sirius Red (PSR) staining, that allows to discern about thin immature collagen fiber (green) typical of type III collagen, and thick mature collagen fiber (red) typical of type I collagen (fig.4a-d). Hyaluronic acid (HA) has been investigated by immunofluorescence as non-collagenous component of ECM (fig. 4e-h). Imaging analysis has been performed on both PSR images and HA immufluorescence.

The former show a decrease in both kinds of collagen in UVA-HDE compared to control at both time points (fig. 4i-l). In particular the difference is more marked at 72 hours for immature collagen, indeed the control has a value of $9.4x10^{-3} \pm 3x10^{-3}$ (pixel $pixel^{-1}$) while the UVA-HDE has a value of $3x10^{-3} \pm 1x10^{-3}$ (pixel $pixel^{-1}$). Interestingly the photoprotected samples have mature and immature collagen amount equal to control, demonstrating the photoprotective action of Dolichos as well as of its positive control retinoic acid.

Amount of synthesized HA quantitatively assessed by imaging analyses show a significant increase of HA in UVA-HDE compared to control (fig.4m). The increase in HA deposition is avoided in the photoprotected samples that maintain the value of control; indeed no statistical difference is assessed between control sample and photoprotected ones, at both time points.

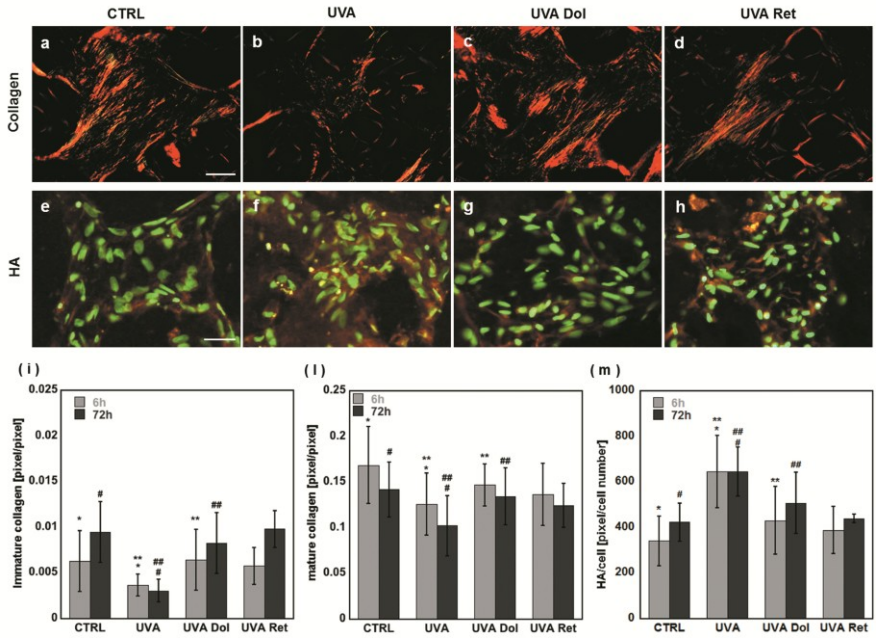

Figure 4:Picrosirius Red staining of 3D_HDE (a-d). Scale bar 50 µm. Immunofluorescence analysis of 3D_HDE: Expression of Hyaluronic Acid (red) and SYTOX® Green (green) (e-h) scale bar 25µm; quantitative analysis of Immature collagen(i) and mature collagen (l) and HA at 6 and 72 hours after UVA exposure

Collagen remodeling in photoexposed and photoprotected samples

The collagen fibrils structure was observed by using MPM that allow to visualize unstained collagen structure by exploiting SHG. By performing (gray-level co-occurrence matrices) GLCM texture analysis [14-16] we evaluated the correlation length as parameter indicating the roughness of the collagen matrix. SHG imaging has been performed on treated and not treated HDE and fibroblast-populated collagen as well, in order to highlight responsiveness and structural difference in collagen organization between endogenous and exogenous ECM. All samples have been observed at the two time points but only images at 72 hours have been shown in figure 5a-h. By comparing the SHG images of HDE (fig. 5a-d) with those of fibroblast-populated collagen (fig. 5e-h) it is possible to note the different organization of the endogenous and

exogenous collagen. In detail, in all images of the fibroblast-populated collagen sample there is a high background noise compared to clear SHG signal, the fibers appear short, thin, loosely packed and with randomly local orientation and it is not possible to observe significant differences between the UVA, not photo-exposed and photo-protected samples. On the contrary in the HDE image is possible to observe an intense SHG signal that displays a denser matrix with collagen bundles much tighter and more organized compared to fibroblast-populated collagen samples. Moreover, in the UVA-HDE sample, the fibrils show marked clumping indicating a loss of the fine structure and structural organization, while the sample treated with retinoic acid and Dolichos have a collagen structure very similar to the control. In order to make such observation objective, correlation curve has been calculated at both time point for all samples and its behavior has been reported in the figure 5(i-l) for sample having endogenous ECM and Figures 5(m-n) for sample having exogenous ECM. UVA-HDEs are characterized by the highest correlation values indicating collagen matrix coarsening due to UVA exposure. In contrast photoprotected sample presents a correlation curve very similar to control. The correlation curves of fibroblast-populated collagen present a completely different behavior. Typical collagen coarsening due to photoaging is not detected indeed the correlation curve of not photoexposed-fibroblast populated collagen appears higher than that of photoexposed-one.

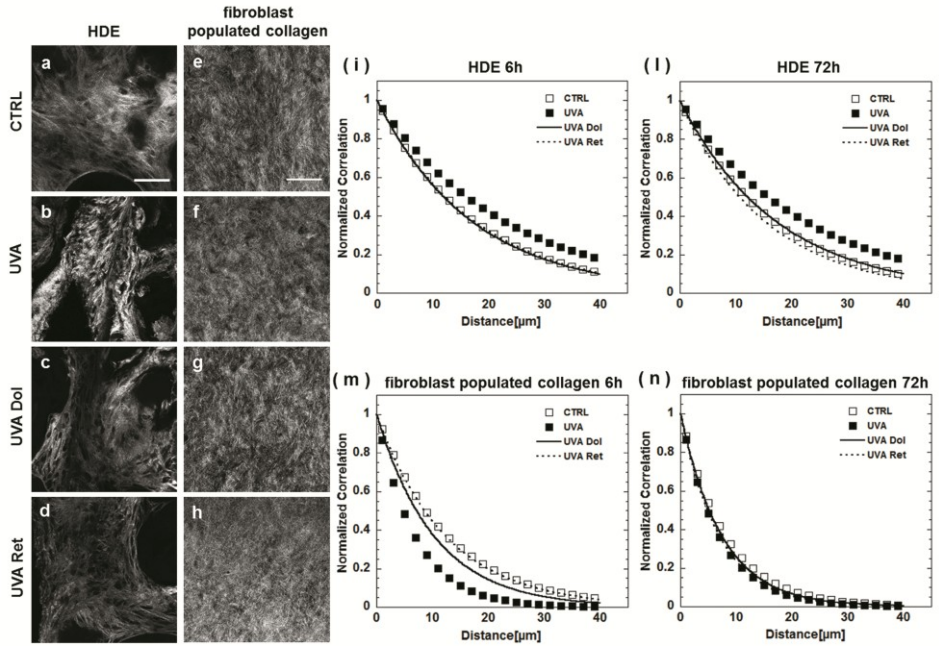

Figure 5: SHG images rispectively of 3D_HDE (a-d) and fibroblast-populated collagen(e-h) at 72 hours after UVA exposure. Scale bar 50µm; Normalized correlation of 3D_HDE after 6 hours(i) and 72 hours (l) of UVA exposure and fibroblast-populated collagen after 6 hours(m) and 72 hours (n) of UVA exposure

In table 1 the correlation length calculated in a windows of 40 µm have been reported: according to the behavior of correlation curve, UVA-HDE presents the highest correlation length at both time points, 23.10 µm ± 6.95 µm and 22.65 µm ± 6.9 µm compared to control that presents values equal to 17.72 µm ± 6.76 µm and 17.14 µm ±5 µm, respectively 6 and 72 hours after photoexposure ($p<0.05$). In the case of Photoprotected HDE its correlation length presents the same value of the control both for UVA-Dol HDE and UVA-Ret HDE. In contrast, the value of the correlation length of photoexposed fibroblast-populated collagen construct decrease compared to control 6.85 µm ± 3.3 µm *vs* 12.69µm ± 9.8µm.

Table 1. Fitting parameters from normalized correlation curves

Type of treatment	Correlation length ± SD HDE (µm)		Correlation length ± SD Fibroblast-population collagen (µm)	
	6 h	72 h	6 h	72 h
CTRL	17.7 ± 6.7	17.1 ± 5	12.6 ± 9.8	8.0 ± 4.8
UVA	23.1 ± 6.9	22.7 ± 6.9	6.8 ± 6.2	6.8 ± 3.3
UVA Dol	17.3 ± 7.2	17.5 ± 5.1	10.3 ± 5.2	7.4 ± 4.4
UVA Ret	17.7 ± 6.5	15.4 ± 2.2	12.4 ± 8.7	6.9 ± 4.0

Abbreviation: SD, standard deviation

Conclusion

In the present chapter, HDE models have been realized to study UVA-induced dermal matrix damage and the efficacy of photoprotecants in preserving the structure and composition of the dermal ECM.

We induced the photodamage with a UVA dose that allowed physiological survival of the model but assured the expression of specific UVA-induced alterations [4].

It is known that UV irradiation during excessive and prolonged sun exposure can cause severe acute damage and also be responsible for long-term effects such as photoaging of the skin. The structural consequences of photoaging are mainly evident in the ECM-rich dermis where key proteins are particularly susceptible to photodamage. Exposure to UVA, in particular, induces extensive changes in the composition and architecture of the ECM-rich dermis [17]. It has been demonstrated that UVA dermal effects do not depend on an epidermal response [4], as consequence since the aim of the present work is to investigate the UVA effect on the endogenous dermis, a dermal equivalent model without epidermis has been produced. It is well known that MMP have an important role in photoaging process [18,19]. In particular, MMP1 acts directly on collagen I. MMP9 acts as a non-specific collagenase, once the collagen has been cleaved by MMP1 it is

further broken by MMP9. According to literature we found an increase of MMP1 and MMP9, and a decrease in the collagen type I and III in the sample UVA-treated. Regarding the photoprotecants, we tested retinoic acid a lipophilic molecule well known for its anti-aging and anti-UVA effects [20], and Dolichos biflorus, a cell culture extract that has been recently demonstrated [9] to protect cellular components from photo-damages due to the presence of flavonoids and their derivatives in its composition. We found that in UVA-Dol and UVA-Ret, MMPs induction is blocked only 72 hours after UVA irradiation. On the other hand, immature and mature collagen synthesis in the same samples was preserved and maintained at the same value of the control both at 6 and 72 hours after UVA irradiation. We hypothesized that Dolichos and retinoic acid due to their antioxidant activity [9] are capable of scavenging the free radicals minimizing the damage to the proteins and in particular preserving the disassembling and the collagen degradation both at 6 and at 72 hours after UVA irradiation, as confirmed also by SHG imaging [21-23] .

Otherwise in fibroblast-populated collagen gel culture, Dolichos as well as retinoic acid blocked MMPs induction both at 6 and 72 hours after UVA irradiation.

We argued that due to the exogenous nature of the ECM in fibroblast-populated collagen gel culture, the antioxidant action of photoprotecants is engaged exclusively in the protection of the cells.

The dynamic interplay between cells and its own ECM plays a crucial role in regulating tissue function and tissue responsiveness to an external stimulus. Previous work demonstrated that the lack of collagen I synthesis in photodamaged dermis was not because of irreversibile damage to fibroblasts collagen-synthetic capacity, but the interaction of fibroblast with a photo-damaged dermis induced a depressed collagen synthesis. Indeed, while in photodamaged dermis collagen fibrils are

shortened, thinned and disorganized in healthy dermis fibrils exists as a highly organized matrix. Normal function of fibroblasts in dermis requires appropriate interactions with collagen fibrils and these interactions cannot be achieved when the fibrils are fragmented [24]. SHG imaging, allowing the visualization and quantification of collagen matrix change also in vivo, is becoming an intrinsic biomarker for evaluating tissue health-status [25].

Our in vitro model, consisting in fibroblasts embedded in their own ECM, is a unique model allowing the study of collagen and its degeneration due to photoaging. Indeed according to study performed *in vivo* on photoaged skin [13], we are able to quantify the collagen structure by using GLCM texture analysis and evaluating the difference between the denser and fine structure fibrils collagen matrix of the normal dermis, and the loss of fine structure and structural organization of the photoexposed dermis. This result could not be reached with the fibroblast-populated collagen gel cultures, that even if widely used as "dermal equivalent", can replicate the photodamage of human dermis, only partially (i. e. cellular level). Indeed, when a GLCM texture analysis was performed on SHG images from fibroblast-populated collagen gel, since only exogenous collagen was present, no typical "dermis-aging behavior" was detected. In other words, when fibroblasts are seeded in exogenous biomatrices, the cross-talk with its extracellular space is limited to basic functions such as: adhesion, migration and traction of collagen fibers [26]. The change in correlation length demonstrated that our model responded to an external stimulus as a real tissue, and this is due to the presence of the cell-synthesized ECM organized in a 3D fashion. Moreover since our HDE is a complex of cell within their own ECM, which is composed not only by collagen but also other proteins, we could also investigate the effect of photoaging on HA production. In previously studies by Tzellos *et al.* [27] the expression of HA in

photoexposed and photoprotected human skin tissue specimens obtained from the same patient, has been investigated. They reported that photoexposed skin was associated with increased levels of fragmented HA having lower molecular mass, as compared with photoprotected skin, indicating that alterations in HA homeostasis are implicated in photoaging. They quantified HA increase both by elisa assay and electrophoresis of the total GAG isolated and purified from photoprotected or photoexposed skin. According to these data, we found an over-production of HA in UVA treated sample while the photoprotected sample maintained the same value of the control, indicating that both Dolichos and retinoic acid were able to protect HA from damage due to UVA. The capability of retinoic acid to both induce sub-epidermal repair zone of new collagen and reduce abundant GAGs present in photoaged skin, were already demonstrated in animal model [28]. The possibility to have an in vitro platform, such as HDE, to investigate the organization and assembly of collagen, as well as deposition of other fundamental components of ECM, presents important consequence not only in dermatology but also in cosmetology science; it opens the possibility to investigate in vitro cosmetic function previously assessable only in vivo. Indeed, in our study we can assess the capacity of Dolichos, not only to protect the dermis from MMPs overproduction and collagen decrease, but we can also to get information about its capacity to protect ECM by collagen coarsening. It is important to point out that collagen synthesis is regulated by interaction between fibroblasts and ECM; in photodamaged skin collagen fibrils are shortened, thinned and disorganized, as consequence fibroblasts are inhibited in synthesizing collagen [8]. This dynamic reciprocity between the cellular and extracellular space is fundamental for the tissue functions and can be obtained only when cells are embedded in their own ECM. In conclusion our system, due to its endogenous nature,

could represent a valuable tool to study tissue status in vitro both at cell and extra-cellular level, respectively. Since in both dermatology and cosmetology science, there is a strong need to replace in vivo model with a more realistic, reliable and cost-effective platform for rapid screening, our study pave the way to the development of a new class of in vitro tissue model that correctly reproduce in composition and organization the extracellular space, leading to the possibility to study in vitro the effects of change of human dermis (e.g. by aging) on selected aspect of both cellular and extracellular components. It is conceivable that a full human skin equivalent could be engineered starting from the dermis equivalent realized and either the effect of an external stimuli (UVR, drug, cosmetics, toxin..) on dermis and epidermis could be studied.

REFERENCES

1. Varani J et al. Inhibition of type I procollagen synthesis by damaged collagen in photoaged skin and by collagenase-degraded collagen in vitro (2001).

2. Fisher GJ, Kang S, Varani J, et al. Mechanisms of Photoaging and Chronological Skin Aging. *Arch Dermatol* 138:1462-70 al (2002).

3. Battie C, Jitsukawa S, Bernerd F, *et al* New insights in photoaging, UVA induced damage and skin types. *Exp Dermatol*, 23:7-12 (2014).

4. Bernerd F, Asselineau D *et al.* UVA exposure of human skin reconstructed in vitro induces apoptosis of dermal fibroblasts: subsequent connective tissue repair and implications in photoaging. *Cell Death Differ* 5:792-802 (1998)

5. Imparato G, Urciuolo F, Casale C, et al. The role of microscaffold properties in controlling the collagen assembly in 3D dermis equivalent using modular tissue engineering. *Biomaterials* 34:7851-61 (2013).

6. Egeblad M, Rasch MG, Weaver VM. Dynamic interplay between the collagen scaffold and tumor evolution. *Curr Opin Cell Biol* 22:697-706 (2010).

7. Iozzo RV, Schaefer L. Proteoglycans in health and disease: novel regulatory signaling mechanisms evoked by the small leucine-rich proteoglycans. *FEBS J* 277:3864-75 (2010).

8. Quan T, Little E, Quan H *et al.* Elevated matrix metalloproteinases and collagen fragmentation in photodamaged human skin: impact of altered extracellular matrix microenvironment on dermal fibroblast function. *J Invest Dermatol* 133:1362-66 (2013).

9. Bimonte M, Tito A, Carola A *et al*. Dolichos cell culture extract for protection against UV damage. *Cosmet Toilet* 129:46–56 (2014).

10. Barbulova A, Apone F, Colucci G Plant Cell Cultures as Source of Cosmetic Active Ingredients. *Cosmetics* 1:94-104 (2014).

11. Nadkarni SK, Mark CP, Park BH *et al*Measurement of collagen and smooth muscle cell content in atherosclerotic plaques using polarization-sensitive optical coherence tomography. *J Am Coll Cardiol* 49:1475-81 (2007).

12. Urciuolo F, Imparato G, Casale C et al. Fabrication of 3D tissue equivalent: an in vitro platform for understanding collagen evolution in healthy and diseased models. Proc. SPIE 8792, 87920K (2013).

13. Cicchi R, Kapsokalyvas D, De Giorgi V *et al.* Scoring of collagen organization in healthy and diseased human dermis by multiphoton microscopy. *J Biophoton* 3:34-43 (2010).

14. Raub CB, Suresh V, Krasieva T, et al. Non invasive Assessment of Collagen Gel Microstructure and Mechanics Using Multiphoton Microscopy *Biophysical Journal* 92:2212–22 (2007).

15. Zhuo S, Chen J, Wu G et al. Quantitatively linking collagen alteration and epithelial tumor progression by second harmonic generation microscopy *AIP* 96:213704-06 (2010).

16. Wu S, Li H; Yang H et al. Quantitative analysis on collagen morphology in aging skin based on multiphoton microscopy *J. Biomed. Opt*. 16,:040502 (2011).

17. Thurstan SA, Gibbs NK, Langton AK *et al.* Chemical consequences of cutaneous photoageing. *Chem Cent J* 6: 34-41 (2012).

18. Fisher GJ, Datta SC, Talwar HS, *et al.* The molecular basis of sun-induced premature skin aging and retinoid antagonism. *Nature* 379:335-338 (1996).

19. Fisher GJ, Wang ZQ, Datta SC, et al. Pathophysiology of premature skin aging induced by ultraviolet light. *N Engl J Med* 337:1419-28 (1997).

20. Fisher GJ, Voorhees JJMolecular mechanisms of photoaging and its prevention by retinoic acid: ultraviolet irradiation induces MAP kinase signal transduction cascades that induce Ap-1 regulated matrix metalloproteinases that degrade human skin in vivo. *J Investig Dermatol Symp Proc*. 3:61-8 (1998).

21. Yaar M, Gilchrest BA. Photoageing: mechanism, prevention and therapy. *Br J Dermatol* 157:874-887 (2007).

22. Gopinath D, Ahmed MR, Gomathi K, *et al.* Dermal wound healing processes with curcumin incorporated collagen films. *Biomaterials* 25:1911-1917 (2004).

23. Mukherjeea PK, Maitya N, Nemaa NK, et al. Bioactive compounds from natural resources against skin aging. *Phytomedicine* 19:64-73 (2011).

24. Fisher GJ, Quan T, Purohit T, et al. Collagen fragmentation promotes oxidative stress and elevates matrix metalloproteinases-1 in fibroblasts in aged human skin. *Am J Pathol* 174:101-14 (2009).

25. Brown E, McKee T, diTomaso E, et al. Quantitative analysis on collagen morphology in aging skin based on multiphoton microscopy. *Nat Med* 9:796-800 (2003).

26. Grinnell F Fibroblast biology in three-dimensional collagen matrices *Trends in Biotech*. 13:264–69 (2003).

27. Tzellos TG, Klagas I, Vahtsevanos K, et al. Extrinsic ageing in the human skin is associated with alterations in the expression of hyaluronic acid and its metabolizing enzymes. *Exp Dermatol* 18:1028-35 (2009).

28. Schwartz E, Kligman LH. Topical treitinoin increase the tropoelastin and fibronectin content of photoaged hairless mouse skin. *J Invest Dermatol* 104:518-22 (1995)

Chapter 4

A human skin equivalent model as in vitro testing platform for bioactive molecules

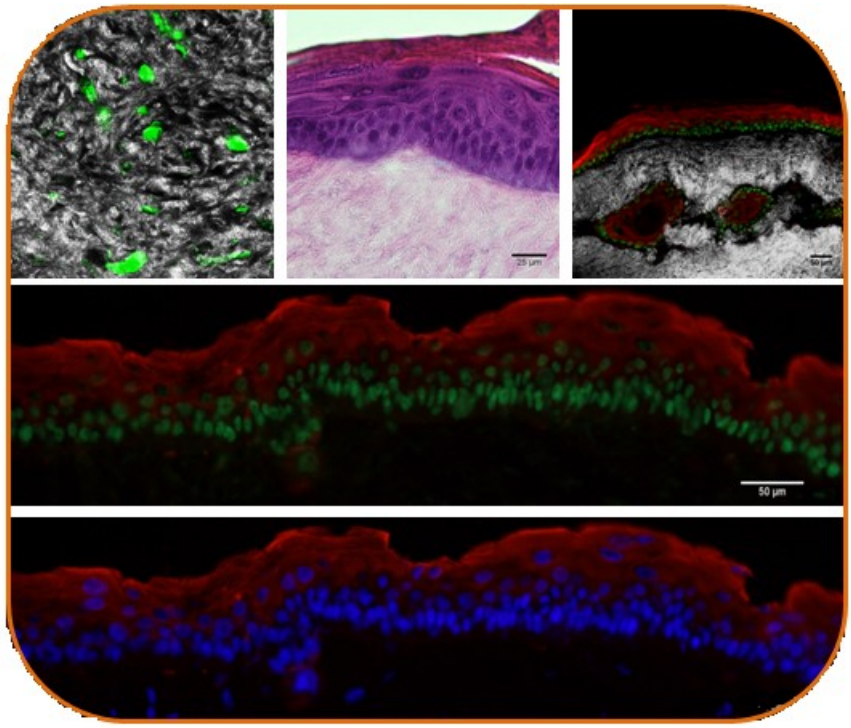

Introduction

The development of effective and alternative tissue-engineered skin replacements to autografts, allografts and xenografts has became a clinical requirement due to the problems related to source of donor tissue and the perceived risk of disease transmission [1].

However, human skin equivalent relevance is correlated not only to their clinical and surgery applications, but also as reliable testing platform alternative to animal testing in the dermo-cosmetical field . The scientific community supports animals, which are subjected to considerable pain and distress during toxicity testing with final results scientifically unreliable because humans and animals can have different reactions to the same chemical. For this reason, animal testing for cosmetics has been banned in the European Union and a new law also strengthens the ban on the sale of products from third countries tested on animals by March 2013 [2](see chapter 1).

To meet these needs, in vitro fabrication of human skin tissue, that mimic the biochemical and morphologic properties of native human skin, known as skin equivalent cultures, has opened new avenues in the study of skin biology.

These skin equivalent models consist mainly of keratinocytes that are cultured on a dermal substitute for approximately two weeks at the air–liquid interface, which allows for epidermal differentiation and development of stratified layers [3-7]. Until now, very scarce importance has been given to the realization of a skin model made up by both dermis and epidermis parts. Great parts of the existing human skin equivalent models used as in vitro testing platform [8-13] have been made up by an epidermis on a polycarbonate mesh or on exogenous matrix. Obviously, this matrix do not mimic the real structure of dermal tissue.

In this chapter, we developed a 3D human skin equivalent model (called 3D HSE) based on endogenous ECM in dermal and epithelial

compartment. We used the dermis equivalent described in the second chapter to seed keratinocytes and performing an organotypic culture in order to realize the final 3D skin equivalent model.

First of all we described the optimal conditions to build up the epidermis and the final skin equivalent, then we demonstrated how the model can be used as testing platform for study photoaging process both at dermis and epidermis level.

MATERIALS AND METHODS

Fabrication of 3D human skin equivalent

The realization of human dermis in vitro is similar to that described in chapter 2.

Briefly, human dermal fibroblasts were sub-cultured into 150 mm Petri dishes in culture medium and maintained at 37 °C, 5% CO_2 and humidity 90%. Dermal microtissue (HD-μTP) were produced by seeding HDF of passages 6-12 on gelatin porous microcarriers with 4% of glyceraldehydes crosslink, in a spinner flask for 9 days and then transferred into the maturation chamber to allow their molding in disc-shaped tissue-construct such as HDE (1 mm in thickness, 5 mm in diameter) as previously described.

Maturation of HDE was carried out until 6 weeks in dynamic conditions by placing the chamber on the bottom of a spinner flask operated at 60 rpm at 37 °C, 5% CO_2 and humidity 90%. The medium was changed every 2 days and at each medium change ascorbic acid was added at a concentration of 50 $\mu g\ ml^{-1}$.

After 6 weeks of culture, under dynamic conditions, the human equivalent dermis has been removed from the maturation chamber and moved to trans-well (Corning Castar 3.0μm pore size tissue culture treated polycarbonate membrane sterile)waiting for seeded with keratinocytes in order to obtain the epithelial layer.

Extraction of keratinocyte from skin biopsy

Skin sample derived from reduction surgery with the informed consent of the patient.

Under sterile conditions, the biopsy was rinsed more times with PBS in order to remove traces of blood, after we put biopsy in PBS/2% pen/strep(P-S) solution at 4° C for about 2h and then we remove hairs from the top and all fat and tissue remnants from the bottom side keeping the biopsy in a cold solution of PBS/1% P-S.

Cut skin into strips of about 3mm width. Transfer strips into new small petri dish, wash with PBS (important: do not use PBS with calcium and magnesium at this step). Incubate skin strips with Dispase solution (2U/mL; about 5-10 ml for 6cm² of skin) that all strips are covered with it; incubate over night on rotating plate to 160 rpm for 16h to 18h.

The day after, check sterility control for contaminations; and control if after 16h the epidermis has removed from dermis (you can see this at the edge where epidermis is partly detached from dermis. If so: stop digestion by transferring skin strips to PBS; if not: incubate for 2 more hours; do not incubate the skin strips for more than 20h in Dispase as this will strongly harm your cells). After transferring the skin strips to PBS, wash them once to stop the Dispase reaction. Separate epidermis from dermis with tweezers. Cut epidermis into small pieces and transfer pieces into preheated in 5mL 0,05% Trypsin/EDTA, wash petri dish with another 5 mL Trypsin/EDTA and transfer it to the tube- Incubate Trypsin/EDTA (with cutted epidermal pieces) for 5 min at 37°C water bath, vortex shortly every 1-2 min (important: the water bath temperature has to be 37°C, therefore do not place large cold flasks into it as this would reduce the temperature). Stop enzyme reaction by adding 1 mL FBS. Resuspend solution for 5 min (plastic single-use pipette) to separate cell clumps Strain solution by transferring it to new tube through cell strainer. Use the same pipette with prepared 10 mL PBS solution to

wash the tube, the single-use pipette and finally transfer solution through cell strainer, too. Centrifuge: 5 min 1200 rpm. Re-suspend cells in culture media and count cells. Seed cells into flasks: 8*10³ cells per cm². After 3 days 2nd medium change (cells should feature characteristic morphology now). Let cells culture up to 80% confluency before detaching and seeding dermis equivalent (not more as keratinocytes will start to differentiate).

The choise of colture medium is important in order to obtain undifferentiated keratinocyte. In this case, we used KGM^{TM}-2, which is based on an optimised formulation and is serum-free. The medium contains the base medium, separate vial of calcium chloride and supplementary mix such as: GA(gentamicin), transferrin, epinephrine, hydrocortisone, insulin, H-egf, BPE (bovine pituitary extract).

Realization of epidermis layer

Before making the keratinocytes seeding of 3D_human dermis equivalent, is carried a coating of fibronectin in order to enhance cell adhesion. Human fibronectina (Sigma Aldrich) is diluted in salt solution of PBS to a concentration of 50 µg/ml than coat the dermis equivalent with a final volume of 50µl for single sample. Allow to air dry, under sterile conditions, for 45 minutes at room temperature. During this time, the culture medium was prepared. In this phase, the culture media contains the base medium with 0.1% GA, 0.1% transferrin, 0.1% epinephrine, 0.1% hydrocortisone,0.1% insulin, 0.1% H-EGF, 0.4% BPE , 5% FBS, 1%P/S and calcium chloride at 0.06µM. Afterwards, the keratinocytes in the plate are detached, so wash the keratinocytes 3 or 4 times with PBS/EDTA 0.01M leaving in contact for a few second and after, trypsinize keratinocyte colonies with trypsin/EDTA for 5 min at 37°C to obtain a single cell suspension. Once cells have detached, gently resuspend them in keratinocyte media, count cells and add the

appropriate number of cells to a 15-mL tube so that there will be enough cells (150.000 cells/insert) to seed onto the desired number of inserts. Centrifuge at 1200rpm for 5 min and. At this time, the cells can be seeded directly onto the dermis equivalent; resuspend the keratinocytes so that they are in the small volume needed for plating onto the matrix. It is important to resuspend cells in a small volume as 150,000 cells will be seeded onto the small surface area of the connective tissue (0.5 cm diameter). Gently dislodge the cell pellet and transfer it to a 1.5-mL sterile Eppendorf tube with a 1-mL plastic pipet. Gently resuspend the cell pellet in the eppendorf tube with a 200-µL pipetman until it is cloudy and well suspended and transfer 3.5 µL of the cell suspension to the center of the dermis equivalent. Do not touch for 10 min to allow cells to begin to attach. Incubate at 37°C for 40–80 min without any media to allow the keratinocytes to fully adhere.

After 3 hours cultures are maintained submerged (fig 1) for 6 days, so the medium was added first on the bottom of the well and after the rest of volume gently into the insert top the keratinocytes. The following day, the medium was change with the only different that the FBS concentration is 3%. The medium was change every two days with the only different that the concentration of FBS switches from 3% (third day after seeding) to 0% (fifth day after seeding). After 6 days of submerged conditions, the cultures are raised to the air/liquid interface for 14 days. In this phase, the culture media contains the base medium with 0.1% GA, 0.1% transferrin, 0.1% epinephrine, 0.1% hydrocortisone, 0.1% insulin, 1%P/S and calcium chloride at 1.88 µM.

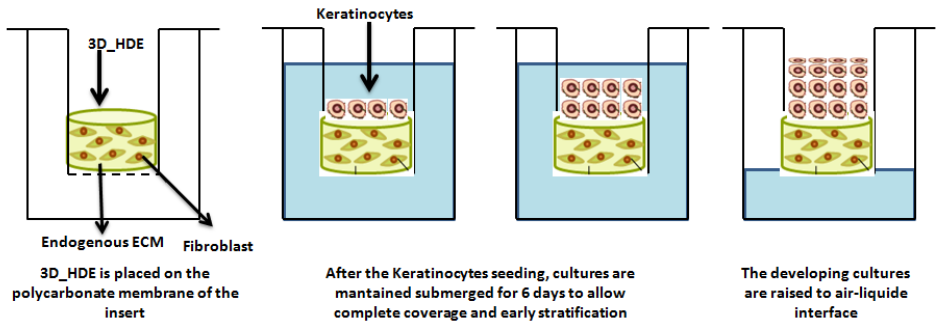

Figure 1: realization of 3D human skin equivalent: phases of keratinization process.

Characterization of human skin in vitro model

In the first part, in order to assess the morphology of the tissue as well as the morphogenesis of epidermal differentiation, were conducted macroscopic analysis through the stereomicroscope (Olympus) and microscopic analysis such as histological and immunofluorescence. After the end of the air-liquide interphase, samples were fixed in 4% paraformaldehyde for 30 minutes at room temperature, wash them in PBS and then placed into a sucrose 2M solution for max 24 hours at room temperature. The day after the samples were included in Tissue Tek (Killik) in a suitable mold and submerged in liquid nitrogen vapors for 1 min and then stored at -80 °C. All samples were cut in slices 5 µm and 50µm in thickness by using criomicrotome. The cut was oriented so as to view the cross section of the samples.ECM composition and morphology along the 3D HSE were assessed by performing histological and immunofluorescence analysis on 5 µm transverse sections of sample and by SHG analysis on 50 µm transverse sections of sample for the assessing of the collagen structure

Histological analyses

Hematoxylin-eosin, picrosirius red staining were performed after hydratation of the sample, finally the sections were mounted with histomount mounting solution (INVITROGEN) on coverslips following

standard procedure by an optical microscope.

Immunofluorescences analyses

For immunofluorescences analyses (IF), the slices were permeabilized with 0.01% Tritox X-100 in PBS/BSA 3% for 1 hour at room temperature. After, the slices were incubated for 3 hours at room temperature with primary antibodies followed by incubation of appropriate secondary antibody for 2 hours at room temperature. Moreover Keratin 10 (K10), Keratin 14 (K14), P63, Ki67 epithelial markers were performed using respectively: keratin 10 polyclonal antibody (diluition 1:500; Covance), keratin 14 polyclonal antibody (diluition 1:1000; Covance), Anti-p63 monoclonal antibody (diluition 1:100;abcam), anti laminin V monoclonal antibody (diluition 1:500; abcam). Every antibody monoclonal were produced in mouse and the polyclonal antibody were produced in rabbit.

The secondary antibodies that we used were: Alexa Fluor 546 goat anti-rabbit IgG (H+L) (diluition 1:500; Life technologies), Alexa Fluor 488 goat anti-mouse IgG (H+L) (diluition 1:500; life tecnologie), Alexa Fluor 546 goat anti-mouse. IgG (H+L) (diluition 1:500; life technologies). The nuclear stain was 4',6-diamidin-2-fenilindolo (DAPI).

Validation of 3D human skin equivalent model as in vitro testing platform for bioactive molecules

As was done on the 3D_human dermis equivalent (see chapter 3), we have used this 3D HSE model as in vitro screening platform of anti –UVA molecular compound. In particular we evaluated successive alteration and recovery of epidermal and dermal morphogenesis with photopretectans after specific UVA-damages. We examined effects of active compound such as formulation of Dolichos extract at 0.01% from topical and topical&systemic application on structure and organization of epidermis and dermis.

In epidermis, the investigations focused on potential effect of UVA exposure on keratinocyte proliferation (Ki67) and p63 expression, since P63 is essential to normal epidermal development.
In dermis, expression of metalloproteases, amount of deposited dermal components and re-organization of collagen matrix after UVA exposure were examined.

UVA source and irradiation

Samples were exposed to UVA radiations by using a UVA lamp in order to simulate solar exposure. The samples were accommodated in transwell, and irradiated in PBS solution for 15 minutes at final power of 20 Joule/cm^2. The UVA lamp was mounted on a stable support allowing an exposure distance of 2 cm from the sample surface.

Sunscreen compound and photoprotection

Dolichos biflorus cell culture extract was previously characterized for its properties to protect skin cell from UV induced damage [14,15] . For our experiments a formulation of Dolichos extract at 0.01% was used. As positive control retinoic acid (1 µM) was used. Treatments with sunscreen were performed 4 hours before UVA exposure by adding 900 µl Dolichos or retinoic acid in the insert of transwell and 5µl on the top of epidermal layer for the topic and systemic application and by adding 5µl on the top of epidermal layer for only topically application. To avoid the formation of phototoxic products, immediately before performing UVA irradiation, culture medium was withdrawn and substituted with fresh PBS solution. Samples were divided into six groups:

- Control (not UVA exposed and sunscreen not treated)
- UVA (UVA exposed and sunscreen not treated)
- UVA Dol T&S (UVA exposed and topic&systemic Dolichos treated)
- UVA Dol Top (UVA exposed and topic Dolichos treated)
- UVA Ret T&S (UVA exposed and topic&systemic retinoic acid

treated)

- UVA Ret Top (UVA exposed and topic retinoic acid treated)

At the end of UVA exposures PBS solution was removed and fresh medium with or without sunscreens was added. The UVA-induced damage and sunscreen protecting effects were evaluated 6 and 72 hours after UVA exposure for all samples.

Histological and immunofluorescences analyses

Collagen morphology was assessed by staining 5µm transverse sample sections with PSR (Sigma Aldrich). Then, stained sample were observed by using an inverted microscope with a digital camera. Quantitative imaging analyses were performed as previously reported (see cap 3) [16,17]. For immunofluorescences analyses, The primary monoclonal antibodies used in this study include: anti-MMP-1 polyclonal antibody (Abcam); anti-MMP-9 monoclonal antibody (Abcam); keratin 10 polyclonal antibody (Covance), Anti-p63 monoclonal antibody (Abcam), anti- Ki67 polyclonal antibody(Abcam). The secondary antibodies used were: Alexa Fluor 568 goat anti-rabbit; Alexa fluor 568 goat anti-mouse; Alexa Fluor 488 goat anti-mouse The cell nuclei were stained by Sytox® Green and 4',6-diamidin-2-fenilindolo (DAPI).). To quantitatively analyze MMPs in each samples, images were processed by using ImageJ® software and the signal was normalized to the cell number. For the analysis of p63, Ki67 and Cells we used the Image J software with the function “Analyze particles”.

Collagen structure by second harmonic generation imaging

The collagen matrix was observed with second harmonic generation _SHG_ imaging. SHG imaging in our samples were performed using a Confocal Leica TCS SP5 II femtosecond laser scanning system (Leica), coupled to a tunable compact mode-locked titanium:sapphire laser (Chamaleon Compact OPO-Vis ,Coherent). The samples were observed

by using λ_{ex} = 840nm (two photons) and λ_{em}=415-425nm. The SHG images, having a size of 200μm x 200μm, were acquired with a resolution of 12bit, 1024x1024 pixel by using a 40X N.A. 1.25 objective. We used Sytox green as nuclear staining. As well as made to the only dermis model (see chapter 3) to quantitatively assess the collagen-related changes, GLCM texture analysis by using ImageJ® plug-in "Texture" on SHG images has been performed [18]. In details, we evaluated the correlation feature for distances ranging from 1 to 200 pixels (corresponding to 1-40 μm) in the horizontal and vertical direction of each optical section that covered a length of interest of 40 μm. In such spatial windows the distance at which the correlation function fell off represented the correlation length of the texture. In particular the correlation curve was calculated *vs.* the neighbor index and the correlation length was obtained by fitting data with an exponential low [18, 19].

Statistical analyses

Data are expressed, as mean ± SD and show the results from three independent experiments. Differences between groups were determined using a nonparametric method, Kruskal-Wallis. Significance between groups was established for $p < 0.05$.

RESULTS AND DISCUSSION

Macroscopic analyses of 3D HSE

The image 2a shows a macroscopic top view of 3D HSE samples in transwell after the air liquid interface It is possible to note the presence of a spot at the center of the sample, indicating the occurrence of a proper epithelial differentiation; likewise in the image 2b is shown a top view of HSE at the stereomicroscope. Also in this case there is the presence of small agglomerates which show the presence of melanin pigments in determining skin color.

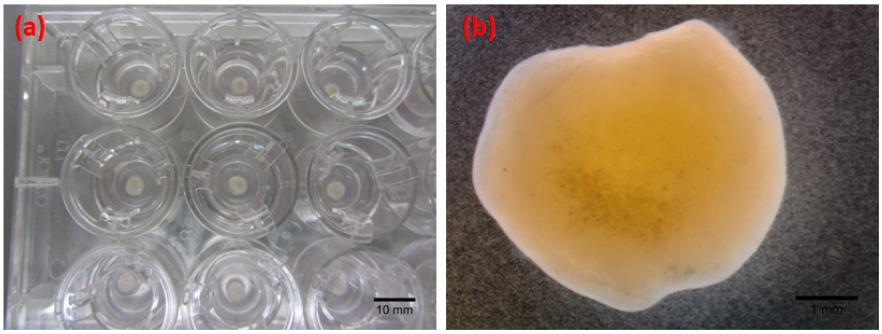

Figure 2 : Macroscopic view of 3D HSE ,(a)top view of HSE in transwell after air-liquid interface. Scale bar 10 mm and (b) top view of sample at stereomicroscope. Scale bar 1 mm

Morphology and composition of skin equivalent

Histological and immunofluorescence analysis; SHG imaging were conducted to observe tissue structure and marker localization of cells in 3D HSE.

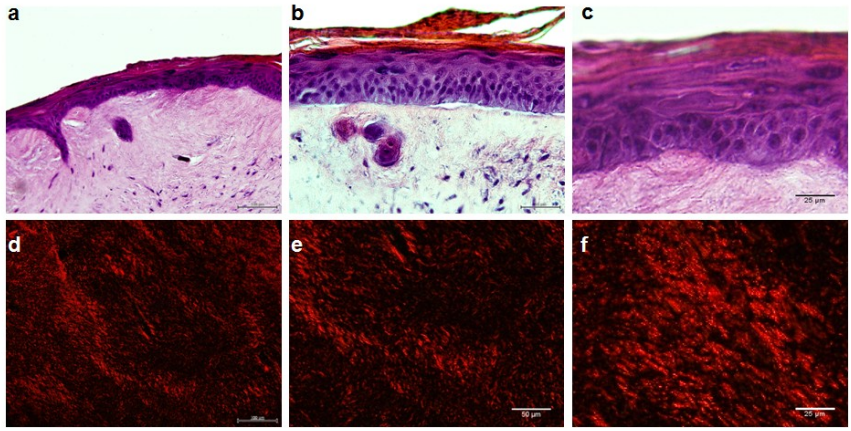

Figure 3: Hematoxylin and eosin and picrosirius red staining of histological section with thick 5 µm of 3D HSE with endogenous dermis . Scale bar: (a,d) is 100 µm,(b, e) is 50 µm and (c, f) is 25 µm.

Due to histological analysis of hematoxylin/eosin (fig 3a,b), it is possible to observe the differentiation of the epithelial layer. Figure 3c, due to the high magnification, highlights the greater degree of epithelium architecture, from the basal layer to the corneum one that present cells without the nucleus.

Moreover both the histological images given from picrosirius red (fig. 3d-f) and SHG imaging (fig.4) confirm the presence of a dense network of collagen matrix with well organized fibers. Furthermore the collagen matrix is very closely to that of native tissue

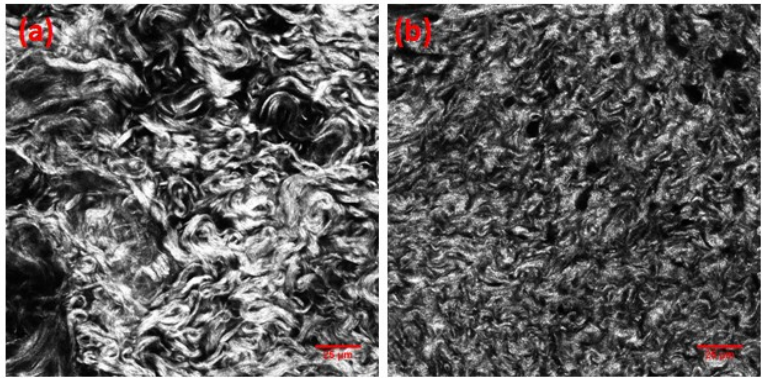

Figure 4: SHG image of human native skin(a) and of 3D HSE (b).
Scale bar 25µm

To evaluate the capacity of primary keratinocytes to generate a correct epidermal tissue on our 3D human dermis equivalent, we detected the epidermal markers by a immunofluorescence analysis.

In figure 5 are shown single markers of each layer which constitute the epithelial tissue starting from the basal layer to the spinus stratum. In figure 5a is shown expression of Keratine 14 (K14) and nuclei with dapi dye. K14 expression is confined to the basal and spinous layer; figure 5b shows the correct morphological expression of transcriptional factor p63 in green in the basal layer; finally in figure 5c it is possible to note the presence of keratin 10 around keratinocytes of the suprabasal layer.

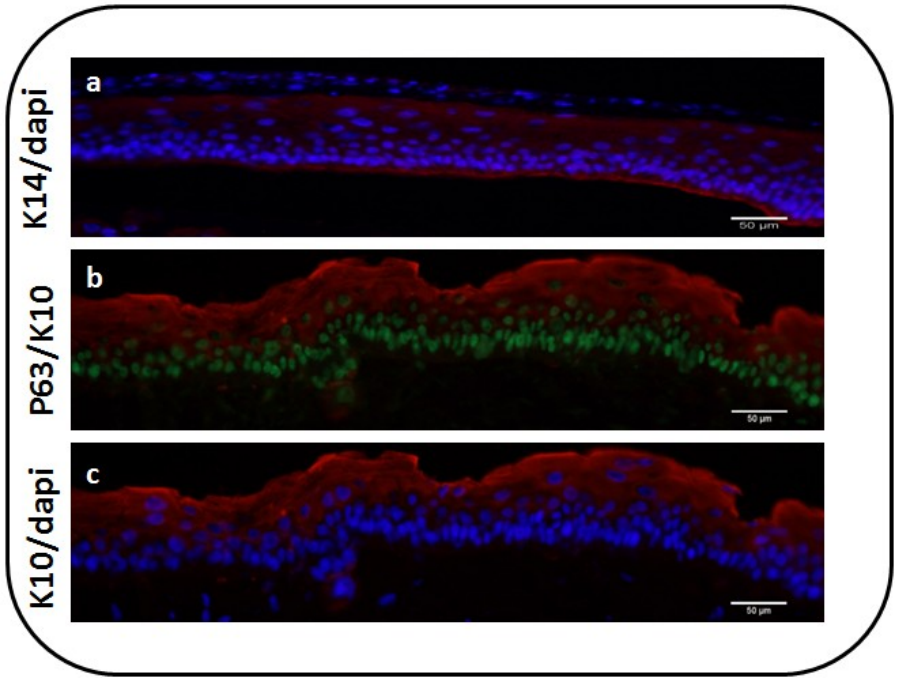

Fugure 5: Immunofluorescence analysis of histological section with thick 5 µm 3D HSE show keratin 14(red) and Dapi as nuclear staining (a); transcriptional factor P63 localized only in the basal layer (green) and keratine 10(red) (b); keratin 10 (red) and Dapi(blue)(c). Scale bar 50 µm.

Alteration and Recovery of epidermal and dermal morphogenesis with photoprotectans compound after specific UVA exposure

Assured that our 3D skin equivalent model is similar to a native tissue from morphological and structural point of view, we assessed whether it was able to respond to an external stimulus like that UVA exposure and specifically we evaluated the action of UVA rays both on derma and epidermis layer.

Effect of UVA and protecants on the dermis layer

Immunofluorescence analyses were performed in order to evaluate the expression of MMP-1 and MMP-9. In figure 6 is shown expression of MMP-1 (fig. 6 a-f) and MMP-9 (fig. 6g-n), 72 hours after UVA irradiation; in detail, the red signal indicates MMPs while the green one indicates the cells stained with Sytox Green.

Quantitative investigations of immunofluorescence images show that MMP-1 (fig.6o) and MMP-9 (fig.6p) per cells in 3D HSE irradiated with UVA but not treated with photoprotectants increased respectively 1.85 and 1.71 times compared to the control samples 6 hours after UVA irradiation and 2.14 and 2.21 times 72 hours after UVA irradiation.

In addition the results showed that the action of Dolichos and retinoic acid are able to decrease the MMPs production both 6 hours to 72 hours bringing its expression to the value of non photo-exposed sample.

Also, it is important to note that the only topical application of photoprotectans fails to protect the samples by the increase of metalloproteinases expression.

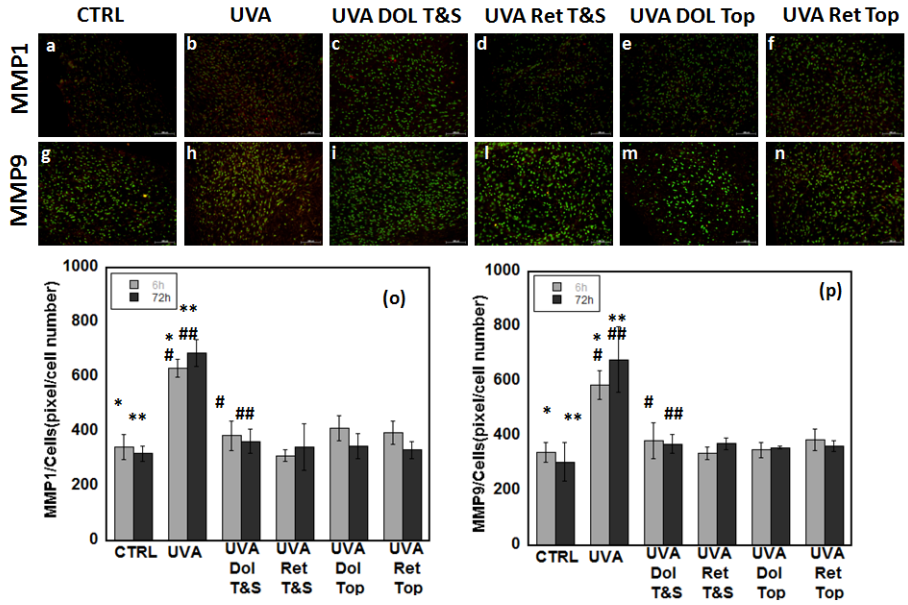

Figure 6 : Immunofluorescence analysis of 3D HSE: Expression of MMP-1 (red) and SYTOX®Green (green) (a-f); Expression of MMP-9 (red) and Sytox (green) (g-n); quantitative analysis of MMP1/Cell(o) and MMP9/Cell (p) at 6 and 72 hours after UVA exposure. Scale bar 100µm.

Collagenous components of endogenous ECM were both investigated in order to evaluate the effects of the UVA irradiation and the anti-aging action of photoprotective. Collagen type I in 3D HSE were investigated by means of Picro Sirius Red (PSR) staining (fig 7 a-f). Quantitative analysis on PRS images showed a decrease of collagen irradiated sample(UVA) compared to the control at both time points (fig 7g). In particular, the irradiated sample(UVA) had a value of $16.1x10^{-2}\pm0.7x10^{-2}$ and $15.9x10^{-2}\pm1x10^{-2}$, respectively at 6 and 72 hours after UVA exposure, while the control sample had a value of $22.6x10^{-2}\pm4x10^{-2}$ and $22.4x10^{-2}\pm3x10^{-2}$. Interestingly, the photoprotected samples, both topic and topic&systemic applications, had collagen amounts equal to the control, demonstrating the photoprotective action of *Dolichos*, as well as of its positive control, retinoic acid.

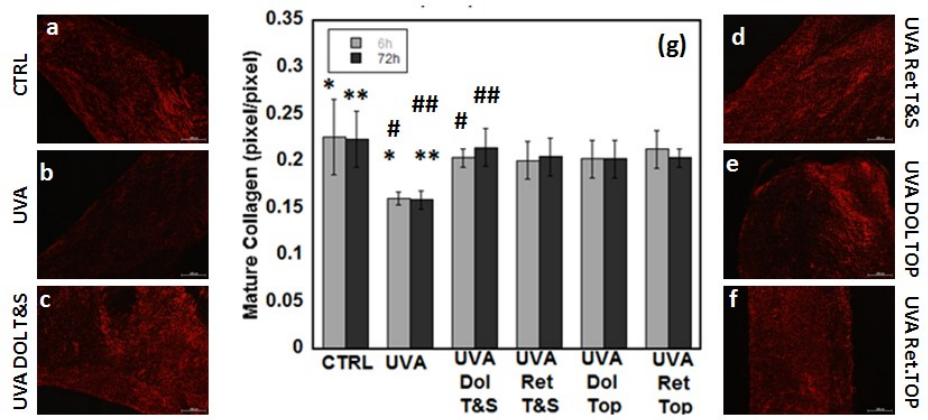

Figure 7: Picrosirius red staining (PRS) of 3D HSE (a-f). Scale bar 100 µm; quantitative analysis of PRS at 6 and 72 hours after UVA exposure(g).

Remodeling of Ecm with and without photoprotectans by SHG signal after UVA irradiation

The remodeling of ECM and in particular of collagen fibrils structure was evaluated by SHG (second harmonic generation) signal using multiphoton microscopy. By performing GLCM texture analysis (gray-level co-occurrence matrices) [20-22] we evaluated the correlation feature or correlation curve as a parameter indicating the fibril and separation of collagen bundles as a as a function of pixel distance. In detail, if the correlation falls off sharply with pixel distance, the collagen matrix presents distinct, linear fibrils as in the case of young and healthy skin; if it remains elevated as pixel distance is increased, the collagen matrix has less defined fibrillar structure as in the case of aging and photoaging skin. We also evaluated a values of correlation (decay) length by fitting the correlation curve with a single exponential decay function. SHG imaging was performed on treated, non-treated 3D HSE model in order to highlight responsiveness and structural differences in collagen organization. All samples were observed at the two time points but only images at 72 hours are shown in figure 8 (a-f).

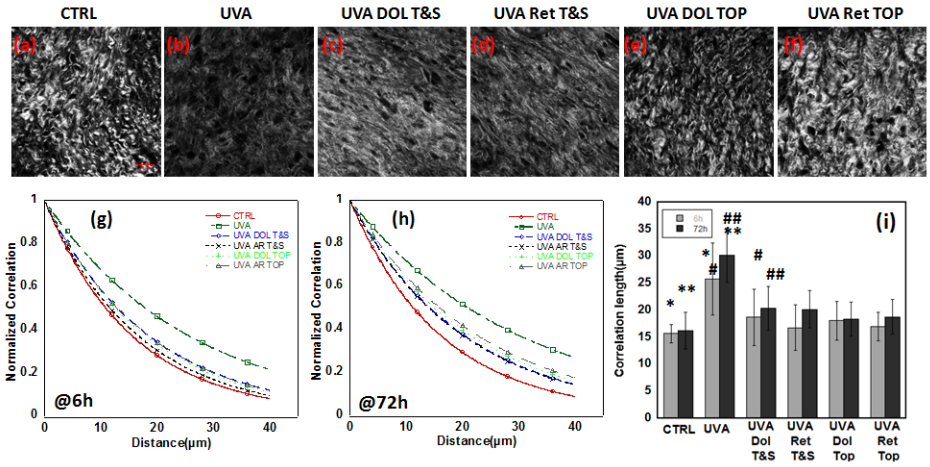

Figure 8 : SHG images 3D HSE model (a-f) at 72 hours after UVA exposure. Scale bar 25µm; Normalized correlation of 3D-HSE after 6 hours(g) and 72 hours (hl) of UVA exposure and correlation length(i).

In the UVA and non treated sample (UVA), the fibrils show marked clumping indicating a loss of the fine structure and structural organization, while the samples treated with retinoic acid and Dolichos have a collagen structure very similar to the control. In order to make such an observation objective, the correlation curve was calculated at both time points for all samples and its behavior was reported in figure 8 (g-h). The UVA samples are characterized by the highest correlation values indicating a collagen matrix coarsening due to UVA exposure. In contrast, the photoprotected sample presents a correlation curve very similar to the control.

The correlation lengths calculated in a window of 40 µm were reported in figure 8i: according to the behavior of the correlation curve, UVA-HDE presents the highest correlation length at both time points compared to the control ($p<0.01$). In the case of photoprotected HDE samples, their correlation length presents the same value of the control.

Effect of UVA and photoprotecants on the epithelial layer

In order to assess the effects of UVA exposure on epithelial layer, immunofuorescences analyzes were conducted; in particular we investigated the expression of respectively Ki67 protein which is strictly associated with cell proliferation and p63 marker. The *p63* gene is a member of the p53 transcription . Expression of p63 is required for proper formation of epithelial tissues. Studies on the transcriptional control of specific genes involved in cell survival, proliferation, differentiation and adhesion have revealed the contributions of p63 to the continuously renewing stratified epithelium.

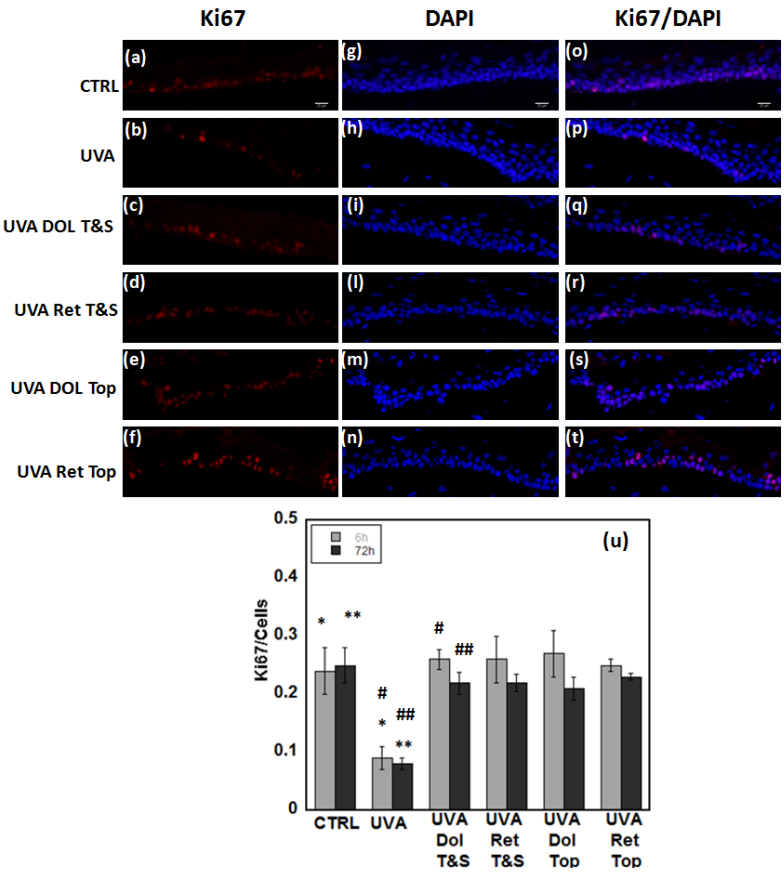

Figure 9: Immunofluorescence analysis of 3D HSE 72 hours after UVA exposure: Ki67 signal(red)(a,f); dapi(blue)(g-n) and merge of Ki67-Dapi)(o-t). Scale bar 25µm; quantitative analysis of Ki67 on cells(u) at 6 and 72 hours after UVA exposure

In figure 9 is shown immunofluorescence analysis of Ki67; in details images (a-f) show ki67 signal; image(g-n) show dapi as nuclear staining and images (o-t) a merge of Ki67 and dapi. Quantitative investigations of immunofluorescence images (image 9-u) have found that Ki67 per cells in 3D HSE irradiated with UVA but not treated with sunscreen (UVA) decreased respectively 2.6 and 3.1 time compared to the control sample 6 hours and 72 hours after UVA irradiation ($p<0.01$); the decrease in Ki67 is avoided in the photoprotected samples(both topic&systemic and topic applications) that maintain the value of control; indeed no statistical difference is assessed between control sample and photoprotected ones, at both time points. Immunofluorescence of P63 marker is shown in image 10.

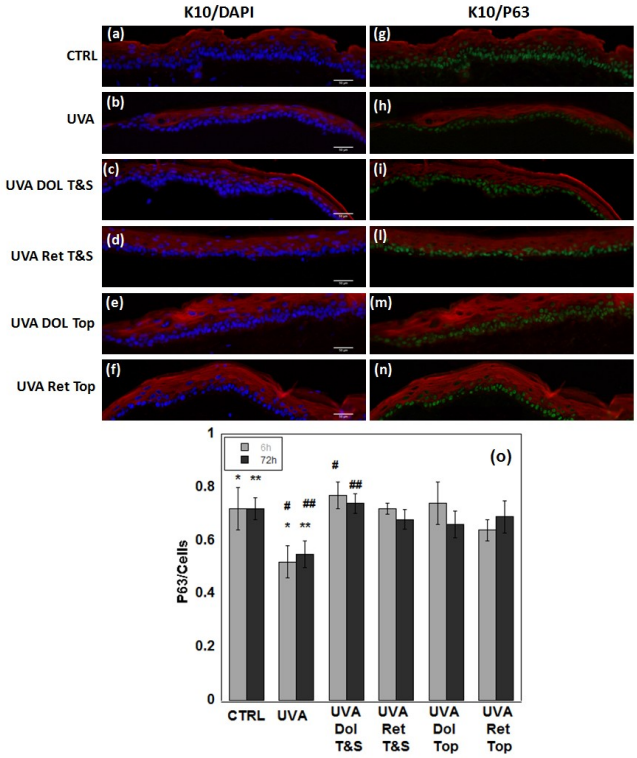

Figure 10: Immunofluorescence analysis of HSE 72 hours after UVA exposure: K10(red) and DAPI(a,f); K10 and P63(green)(g-n). Scale bar 50µm; quantitative analysis of p63 on cells (o) at 6 and 72 hours after UVA exposure.

The images shows the merge of K10 (keratin 10, marker of suprabasal layer) and P63 (fig10 a-f) and the merge of K10 and P63 (fig 10 g-n) at 72 hours after UVA exposure.

Quantitative investigation of p63 (fig 10o) has shown that the action of the UVA irradiation tends to decrease the number of basal stem cells given from the decreases of p63 marker ($p < 0.01$) both at 6h and 72 hours of UVA exposure; instead of in the samples treated with photoprotectans, the expression of P63 on total cells is more similar to the control sample both topic and topic&sistemic application.

Conclusion

In the present chapter, human skin equivalent model have been realized based on endogenous ECM in dermal and epithelial compartment. After a first morphological characterization which showed that our in vitro model has characteristics similar to a native tissue, we validated it as in vitro testing platform for biactive molecules. In details, we studied UVA induced dermal and epithelial damage and the efficacy of photoprotecants in preserving the structure and composition of the tissue. We rated the photodamage provided by the UVA dose that allowed physiological survival of the model but assured the expression of specific UVA-induced alterations [23]. Exposure to UVA, in particular, induces extensive changes in both the composition and architecture of the ECM-rich dermis [24] and in the dermis-epidermis crosstalk. It has been established that UVA radiation, in epithelial layer, caused effects on keratinocytes decreasing expression of the proliferation marker Ki-67 [25] and induced apoptotic pathway, proving that down-regulation of p63 in response to UVA is important to epidermal apoptosis [26]. As regards the UVA damage on dermal compartment, it is well known that MMP have an important role in photoaging process [27,28]. In particular, MMP1 acts directly on collagen I. MMP9 acts as a non-specific

collagenase, once the collagen has been cleaved by MMP1 it is further broken by MMP9. According to literature we found a decrease of both Ki67 and P63 in the sample UVA-treated, both at 6 and 72 hours after UVA exposure, proving that epidermal keratinocytes undergo apoptosis in response to UVA irradiation and loss their stemness. Moreover, we found an increase of MMP1 and MMP9, and a decrease in the collagen type I and III in the UVA sample. These results were also confirmed by the texture analysis performed on SHG images with GLCM which have demonstrated the difference between the denser and fine structure fibrils collagen matrix of control sample, and the loss of fine structure and structural organization of UVA treated sample. Regarding the photoprotecants, we tested retinoic acid a lipophilic molecule well known for its anti-aging and anti-UVA effects [29], and Dolichos biflorus, a cell culture extract that has been recently demonstrated [14] to protect cellular components from photo-damages due to the presence of flavonoids and their derivatives in its composition. We have used two different application of these photoprotecans; only topical application (ie only on the epidermis layer) and both topical & systemic application (both in the dermis that in the epithelium). The choise of 2 routes of administration may be linked on specific penetration potential of photochemicals, or on epidermis barrier function and also on keratinocytes absorption metabolization process.

In both applications, we found a measurable improvement in tissue viability. In fact, the level ofKi67 and P63 are similar to not photoexposed sample proving their antioxidant activity on scavenging the free radicals minimizing the cellular damage. Furthermore, MMPs induction is blocked after UVA irradiation and, immature and mature collagen synthesis was preserved and maintained at the same value of the control both at 6 and 72 hours after UVA irradiation. These results showed that the only topical application fails to protect the tissue ,in both dermal and epithelial

layer from UVA damage; demonstrating the importance of having an adequate dermis/epidermis crosstalk; and to have a dermis matrix which is not inert, but which is also remodels thanks to the stimuli it receives from the epidermis. In conclusion, the possibility to have an *in vitro* platform, such as uman skin model, to investigate the action of external stimuli such as UVA exposure, presents important consequence not only in dermatology but also in cosmetology science; it opens the possibility to investigate *in vitro* cosmetic function previously assessable only *in vivo*. Also we hypothesized that the human skin model realized could be used not only in vitro but also *in vivo* as skin substitute in clinical application.

REFERENCES

1. Sunita Nayak et al. Skin Equivalent Tissue-Engineered Construct: Co- Cultured Fibroblasts/ Keratinocytes on 3D Matrices of Sericin Hope Cocoons PLOS ONE Volume 8,Issue 9 (2013)

2. http://www.theecologist.org/how_to_make_a_difference/campaigning_the_basics/1329786/take_action_to_end_cosmetic_testing_on_animals.html

3. Pruniéras M, Régnier M, Woodley D. Methods for cultivation of keratinocytes with an air-liquid interface. J Invest Dermatol. 81:28s–33s. [PubMed: 6190962] (1983);

4. El Ghalbzouri A, Gibbs S, Lamme E, Van Blitterswijk CA, Ponec M. Effect of fibroblasts on epidermal regeneration. Br J Dermatol. (2002-a); 147:230–43. [PubMed: 12174092]

5. El Ghalbzouri A, Lamme E, Ponec M. Crucial role of fibroblasts in regulating epidermal morphogenesis. Cell Tissue Res310:189–99. [PubMed: 12397374] (2002b).

6. El Ghalbzouri A, Siamari R, Willemze R, Ponec M. Leiden reconstructed human epidermal model as a tool for the evaluation of the skin corrosion and irritation potential according to the ECVAM guidelines. Toxicol In Vitro.; 22:1311–20. [PubMed: 18474418] (2008)

7. Stark HJ, Szabowski A, Fusenig NE, Maas-Szabowski N. Organotypic cocultures as skin equivalents: A complex and sophisticated in vitro system. Biol Proced Online6:55–60. PubMed: 15103399] (2004a).

8. A de Brugerolle de Fraissinette, V. Picarles et al., Cell Biol Toxicol., 15:121-135, 1999.

9. F. Bernard, C. Barrault et al., Cell Biol Toxicol., 16(6):391-400, 2000

10. D Lelièvre, P. Justin, et al., Tox. In Vitro, 21(6):977- 995, 2007

11. ECVAM. ESAC Statement, Corrosion Testing, 2000 http://ecvam.jrc.it/ft_doc/EpiDerm_statement.pdf

12. H. Spielmann, S. Hoffmann et al., ATLA 35: 559–601, 2007

13. H. Kandárová, P. Hayden et al., ATLA 37:671–689, 2009

14. Bimonte M, Tito A, Carola A *et al*. Dolichos cell culture extract for protection against UV damage. *Cosmet Toilet* 129:46–56 (2014).

15. Barbulova A, Apone F, Colucci G Plant Cell Cultures as Source of Cosmetic Active Ingredients. *Cosmetics* 1:94-104 (2014).

16. Imparato G, Urciuolo F, Casale C, et al. The role of microscaffold properties in controlling the collagen assembly in 3D dermis equivalent using modular tissue engineering. *Biomaterials* 34:7851-61 (2013).

17. Nadkarni SK, Mark CP, Park BH *et al*Measurement of collagen and smooth muscle cell content in atherosclerotic plaques using polarization-sensitive optical coherence tomography. *J Am Coll Cardiol* 49:1475-81 (2007).

18. Urciuolo F, Imparato G, Casale C et al. Fabrication of 3D tissue equivalent: an in vitro platform for understanding collagen evolution in healthy and diseased models. Proc. SPIE 8792, 87920K (2013).

19. Cicchi R, Kapsokalyvas D, De Giorgi V *et al.* Scoring of collagen organization in healthy and diseased human dermis by multiphoton microscopy. *J Biophoton* 3:34-43 (2010).

20. Raub CB, Suresh V, Krasieva T, et al. Non invasive Assessment of Collagen Gel Microstructure and Mechanics Using Multiphoton Microscopy *Biophysical Journal* 92:2212–22 (2007).

21. Zhuo S, Chen J, Wu G et al. Quantitatively linking collagen alteration and epithelial tumor progression by second harmonic generation microscopy *AIP* 96:213704-06 (2010).

22. Wu S, Li H; Yang H et al. Quantitative analysis on collagen morphology in aging skin based on multiphoton microscopy *J. Biomed. Opt*. 16,:040502 (2011).

23. Bernerd F, Asselineau D *et al.* UVA exposure of human skin reconstructed in vitro induces apoptosis of dermal fibroblasts: subsequent connective tissue repair and implications in photoaging. *Cell Death Differ* 5:792-802 (1998)

24. Thurstan SA, Gibbs NK, Langton AK *et al.* Chemical consequences of cutaneous photoageing. *Chem Cent J* 6: 34-41 (2012).

25. M. Badawy Abdel-Naser, Konstantin Krasagakis et al. Direct effects on proliferation, antigen expression and melanin synthesis ofcultured normal human melanocytes in response to UVB and UVA light. Photodermatol Photoimmunol Photomed; 19: 122–127(2003)

26. Kristin M. Liefer, Maranke I. Koster et al. Down-Regulation of p63 Is Required for Epidermal UV-B-induced Apoptosis. CANCER RESEARCH 60, 4016–4020, (2000)

27. Fisher GJ, Datta SC, Talwar HS, *et al.* The molecular basis of sun-induced premature skin aging and retinoid antagonism. *Nature* 379:335-338 (1996).

28. Fisher GJ, Wang ZQ, Datta SC, et al. Pathophysiology of premature skin aging induced by ultraviolet light. *N Engl J Med* 337:1419-28 (1997).

29. Fisher GJ, Voorhees JJMolecular mechanisms of photoaging and its prevention by retinoic acid: ultraviolet irradiation induces MAP kinase signal transduction cascades that induce Ap-1 regulated matrix metalloproteinases that degrade human skin in vivo. *J Investig Dermatol Symp Proc*. 3:61-8 (1998).